IEEE Access
Multidisciplinary ⋮ Rapid Review ⋮ Open Access Journal

Received 5 February 2024, accepted 27 February 2024, date of publication 25 March 2024, date of current version 11 April 2024.

Digital Object Identifier 10.1109/ACCESS.2024.3380013

RESEARCH ARTICLE

A New Technique of FSS-Based Novel Chair-Shaped Compact MIMO Antenna to Enhance the Gain for Sub-6GHz 5G Applications

M. Y. ZEAIN[1], MAISARAH ABU[1], AYMAN A. ALTHUWAYB[2], (Member, IEEE), HUSSEIN ALSARIERA[1], AHMED JAMAL ABDULLAH AL-GBURI[1], (Senior Member, IEEE), ALI ABDULATEEF ABDULBARI[3], AND ZAHRILADHA ZAKARIA[1], (Senior Member, IEEE)

[1]Faculty of Electronic and Computer Technology and Engineering (FTKEK), Center for Telecommunication Research and Innovation (CeTRI), Universiti Teknikal Malaysia Melaka (UTeM), Durian Tunggal, Malacca 76100, Malaysia
[2]Electrical Engineering Department, Engineering College, Jouf University, Sakaka 72388, Saudi Arabia
[3]Department of Communication Engineering, University of Technology, Iraq, Baghdad 10066, Iraq

Corresponding author: Zahriladha Zakaria (zahriladha@utem.edu.my)

This work was supported in part by the Faculty of Electronics and Computer Technology and Engineering (FTKEK), Universiti Teknikal Malaysia Melaka (UTeM), under Grant JURNAL/2022/FTKEK/Q00086; in part by Rogers Corporation. The authors extend their appreciation to the Deputyship for Research & Innovation, Ministry of Education in Saudi Arabia for funding this research work through the project number 223202.

ABSTRACT This paper introduces a new compact Chair-shaped MIMO antenna with two radiating elements and a single layer of frequency-selective surface (FSS) for 5G Sub-6GHz communication systems. They use two techniques, Parasitic element, and (FSS), for isolation and gain enhancement, respectively. The 1 × 2 MIMO antenna using a coplanar waveguide (CPW) fed. Moreover, an FSS array structure consisting of (a 68-unit) Square-shaped structure with Circular Slot (SCS) shaped cells is employed using a new technique (Surround Technique) to enhance the gain and isolation between the elements of the MIMO antenna. The proposed MIMO antenna system is printed on a Rogers 4350B substrate with a thickness of 0.508 mm. The antenna's performance is evaluated using S-parameters, radiation properties, and MIMO characteristics. The MIMO antenna system works in the Sub 6-GHz 5G band, which ranges from 3 to 6 GHz. Adding the FSS layer enhances the MIMO's antenna gain to a peak measured gain of 7.96 dBi and it also improves the MIMO antenna's isolation. The performance metrics of the proposed MIMO antenna were also investigated, including measures values of ECC = 0.004, DG = 9.99 dB, CCL = 0.2 bit/s/Hz, MEG = -3.13 dBi, and TARC = > 0dB exhibits advantageous antenna characteristics. The observed radiation characteristics of the suggested MIMO antenna system indicate its suitability for the upcoming 5G communication systems.

INDEX TERMS Multiple-input–multiple-output (MIMO) antenna, 5G, frequency selective surface (FSS), gain enhancement, isolation, mutual coupling.

I. INTRODUCTION

MIMO is a wireless technology that improves the performance of wireless communication systems by utilizing multiple antennas on both the transmitter and receiver sides. MIMO can increase the data rate, reliability, and capacity of wireless communication systems without requiring more power or spectrum. MIMO is used in many different types of wireless communication systems, and it is an essential part of 5G and future wireless communication systems [1], [2].

The associate editor coordinating the review of this manuscript and approving it for publication was Jiankang Zhang.

For the MIMO antenna to perform optimally, the signals received by each antenna should have a low correlation. This requires the antenna ports to have a low mutual coupling. However, in small devices with closely spaced antennas, achieving such low mutual coupling is typically challenging [3]. The mutual coupling between antennas induced by the surface on the ground plane leads to an increase in the correlation between the received signals, which reduces the diversity gain and channel capacity of the system [4].

Achieving high isolation between MIMO antenna elements is a major challenging factor in designing MIMO antennas [5], [6], [7]. Many different techniques have been developed to reduce mutual coupling to date [8], such as neutralization line [9], [12], Decoupling network [13], [14], and Parasitic or slot element [8]. Printed parasitic or slot element antennas are a type of antenna that uses two different modes of operation to create a wide range of frequencies that can be transmitted. they reduce the mutual coupling, by coupling the two types of waves together, either on the radiating patch of the antenna or on the ground plane. This is done by creating an additional coupling path that opposes the signal from the other coupling path. This technique reduces the overall level of mutual coupling or minimizing interference between the antennas. Parasitic or slot element antennas are not connected to the main antenna in any way, and they can be made in a variety of different shapes, including resonators, floating stubs, and shorted stubs [13]. In addition, parasitic or slot antennas are easy to design, small in size, and can be easily manufactured using either printed circuit board (PCB) technology or waveguides [8]. Electromagnetic Band Gap (EBG) is another method used in [15], while Split Ring Resonators (SRRs) are used in [16], Complimentary Split Ring Resonators (CSRRs) in [17], and Defected Ground Structure (DGS) in [18].

FSS techniques can enhance the isolation between antennas, but they are not typically compatible with low-profile structures and can affect the radiation pattern of the antennas. However, FSS techniques can be used between Dielectric Resonator Antennas (DRAs) positioned in the H- plane by using SRRs cells array employed in the E - plane. By modelling the SRRs formation, it is possible to achieve bandstop functionality within the frequency band of the antenna [18], [19], [20]. Moreover, one of the challenges facing researchers in 5G wireless communication is developing compact MIMO antennas that offer both high gain and isolation for Sub6-GHz 5G and NR spectrums. These spectrums are extensively utilized and valued for their wide adoption and ability to provide seamless coverage [7], [12], [21], [22]. Compact MIMO antennas with high gain and isolation can improve the performance and coverage of wireless communication systems, while also reducing the cost of deploying antennas. As a result, researchers are focusing on developing such antennas for wireless terminals and access points [23], [24], [25].

A four-port MIMO antenna with an X-shaped isolating block is described in [26]. The antenna has four feeding monopoles arranged symmetrically and orthogonally in the cavity opening and measures ($129.5\times$ $129.5\times$ 28.2 mm^3); in size. The X-shaped isolating block is placed in the cavity's centre to improve port isolation. The X-shaped technique achieved 16 dB of isolation while maintaining high gain. A 6-port antenna with a diameter of 83 mm is also presented in [27]. The 10-port MIMO antenna proposed in [28] has a total size of $\pi \times 228.85^2 \times 37.27$ mm^3. However, the systems in [26], [27], and [28] are large, and the tendency to increase the number of ports has led to complex designs. In [29], proposed a new antenna design that uses four parasitic resonators to reduce the size to become ($42.5\ mm \times 42.5\ mm \times 18\ mm$), lower the Q-factor, and improve the impedance matching. However, the proposed antenna has an isolation of 14 dB with frequency band of (3.38 GHz - 5.1 GHz). In [30] parasitic decoupling technique was used to enhance the isolation of 4 elements MIMO antenna Array printed on a 200×200 mm substrate of RO4350 Rogers. The isolation improved with 15 dB and 26 dB (from -13 dB to -28 dB and -8dB to -34 dB), respectively. Nevertheless, this paper emphasized the limited frequency range of operation (2.33 GHz – 2.43 GHz) for the MIMO antenna. The MIMO antenna was found to have a bulky size, which may pose practical challenges in certain applications. In [31], the use of parasitic elements to improve MIMO antenna performance is investigated in this paper. The addition of multiple square parasitic elements near each rectangular patch element affects the electromagnetic field distribution and reduces the mutual coupling. As a result, the bandwidth and the gain are enhanced. In both H and E planes ($80\ mm \times 50\ mm$) and ($60\ mm \times 60\ mm$) respectively, the two MIMO antennas are coupled. With a relatively 3.8 dBi of low gain and bandwidth of 0.8 GHz (5.0 GHz - 5.8 GHz), the isolation achieved in both planes is more than 20 dB. Additionally, some of the designs in [23], [29], [30], and [31] have a narrow bandwidth or are not within the band of the 5G New Radio (NR) spectrums ($n77/n78/n79$) and Sub6-GHz 5G. Their resonance frequencies are as follows (5.2 GHz - 5.65 GHz), (3.38 GHz - 5.1 GHz), (2.38 GHz - 2.42 GHz) and (5.0 GHz - 5.8 GHz).

Metamaterials are a type of artificial material that can be designed to have specific electromagnetic (EM) properties [7], [32], [33]. These properties can be used to improve the performance of MIMO antennas in terms of gain and isolation between MIMO antenna elements [34], [35]. Multiple resonances are provided by a dual Folded Monopole antenna (FMA) system measuring ($70\ mm \times 50\ mm$). To address the issue of mutual coupling between 2×2 MIMO antenna elements, a square patch of FSS used as decoupling structure. The FMA system operates at the following frequencies (2.4 GHz - 2.48 GHz), (2.91 GHz - 3.49 GHz), (3.27 GHz - 3.97 GHz), (3.4 GHz - 3.8 GHz), (5.15 GHz - 5.85 GHz). However, the

complex FMA system provides a low efficiency, and it does not cover all sub-6GHz 5G bands [35].

The authors designed a low-profile MIMO antenna with two elements on a single substrate. To enhance the isolation between the two elements, they used Metasurfaces (MS) or parasitic elements positioned around the antenna radiators. While these antennas demonstrate a favorable characteristics such as low profile and high isolation, they exhibited limitations in terms of gain and bandwidth [23], [32].

To reduce the mutual coupling between the two elements MIMO antenna, a dual-band-stop FSS and metal wall are used. The frequency range of the proposed MIMO antenna is (4 GHz - 5.3 GHz) with a height of 21 mm. The 40 × 40 mm MIMO antenna has a low gain of 4 dBi and low efficiency [36]. Huang [37] uses an FSS to decouple two antennas, which means to prevent them from interfering with each other. The FSS is placed between the antennas and is designed to let one frequency band pass through while blocking the other. This ensures that the radiation patterns of the antennas are not affected and that they can operate independently. In addition, Sufian et al. [7] uses an MS layer to minimize the size and profile of an antenna patch while maintaining high gain and isolation. An MS layer is positioned directly on the antenna patch with no air gap between them. However, the systems in [7] and [37] are large and have poor operational bandwidth, which limits their use in real-world 5G NR spectrum or Sub-6 GHz 5G applications.

The use of a phase gradient FSS in a low-profile Fabry-Perot cavity configuration is proposed as a new method for decoupling MIMO antennas. The efficacy of this method is showcased through the design of a 2 elements MIMO antenna system operating at (5.25 GHz) [38]. The authors of [25]; propose a four-port MIMO antenna that uses two phase-gradient an (FSSs) as a superstrate. The FSSs are placed on both sides of the substrate. Additionally, two cylindrical Dielectric Resonator Antennas (cDRAs) are placed at the top and bottom of the substrate to achieve high isolation between the antenna ports. However, these 2 × 2 in [38] and 4 ×4 in [25] MIMO antennas operate at (5.15–5.35 GHz) with a large size and narrow bandwidth, which restricts their suitability for wider applications in 5G bands. The authors of [39] suggested a multiband MIMO antenna with an MS reflector to improve the gain and isolation. They presented two MIMO antenna elements with an MS measuring $83.2 \times 83.2 \times 13.2\ mm^3$. However, the gain improvement using the MS in [39] is only 0.8 dBi, and it exhibits a narrow bandwidth. Furthermore, the large dimension of the antenna is not compatible with the working spectrum and MIMO elements, limiting its practical applicability. Reference [40] proposes a stacked antenna array design using FSS separation that can operate in three sub-6 GHz 5G bands: (0.69 GHz - 0.96 GHz), (1.8 GHz - 2.7 GHz), and (3.3 GHz - 3.8 GHz). The array is relatively large, with dimensions of 200 × 200 × 0.638 mm. It achieves multi-band operation by stacking antennas for different frequency bands on top of each other which are the Middle Band and High Band together above the Low Band. However, this approach requires multiple feeding cables, is complex to design, and does not cover all sub-6 GHz 5G bands. Another approach to designing multi-band MIMO antennas is to use metamaterial unit cells that are placed between two MIMO elements to achieve high isolation between antenna ports [24], [25], [41]. However, this approach also has limitations to be used between the number of MIMO elements and gain enhancement. Additionally, the antennas in [24] and [25], operate in narrow bandwidths, which is not covering the Sub-6GHz 5G bands.

This work proposes a new, compact two-element Chair-shaped MIMO antenna design for sub-6 GHz 5G communication that addresses the limitations of the existing antenna designs discussed above. The new compact MIMO antenna design uses a parasitic element and a single layer of FSS for isolation and gain enhancements, respectively. For the gain enhancement of the suggested MIMO antenna, the single-element antenna is modified into a 2-elements MIMO antenna structure. The 2-elements MIMO antenna is fed by a coplanar waveguide (CPW). To further reduce the coupling effects between the MIMO elements, a parasitic element is added between them. To enhance the gain of the suggested MIMO antenna, Square-shaped structures with Circular Slot (SCS) shaped cells are placed behind them. An FSS of periodically patterned 10 × 8 (Full cells FSS array), enhanced the gain but affected the bandwidth of the suggested MIMO antenna. in addition, the Surrounding Technique (ST) is a new technique used on the FSS array to maintain wideband coverage and the compact dimensions of the suggested MIMO antenna. The number of unit cells of the FSS array becomes 68 unit cells by using the new technique (ST).

The developed MIMO antenna system exhibits notable features such as high gain, wideband coverage, slightly enhanced isolation (−11.55 dB) − (−12 dB) and compact dimensions. The miniaturized design includes a short end–to–end gap of $0.075\lambda_o$(in electrical dimension), which is 5 mm between the adjacent antenna radiators at the centre frequency of (4.5 GHz). The final size of the proposed compact MIMO antenna without an FSS array is 19×43× 0.508 mm ($0.285\lambda_o \times 0.645\lambda_o \times 0.007\lambda_o$). Moreover, the final size of the proposed MIMO antenna system, including the FSS array, is 117.50 mm × 94.90 mm × 30 mm where it's equal to ($1.762\lambda_o \times 1.423\lambda_o \times 0.45\lambda_o$)(in electrical dimension). The FSS significantly enhances the gain of the MIMO antenna, with 7.97 dBi of the peak gain value after using the FSS array. In addition, the enhancement in isolation is attained after introducing the parasitic element and FSS array for the MIMO antenna respectively. The suggested MIMO antenna system covers the Sub-6GHz 5G frequency band (3 GHz - 6 GHz), supporting an Unmanned Aerial Vehicle (UAV) at (5.7 GHz - 5.8 GHz), Cardiac pace marker at (5.8 GHz), Wearable antenna at (4.4 GHz - 5 GHz),

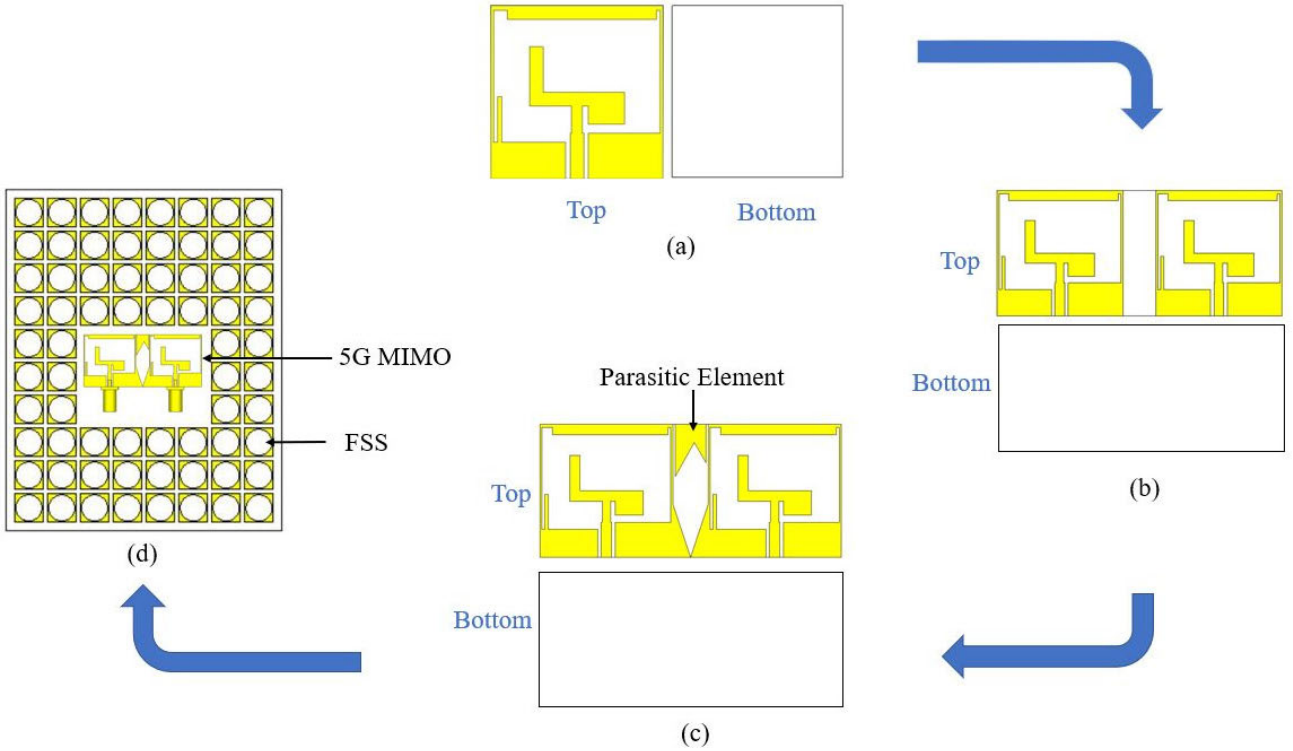

FIGURE 1. Stepwise design progression (a) Single antenna, (b) 2 × 2 elements MIMO with decoupling technique, (c) 2 × 2 MIMO antenna with parasitic element technique, (d) MIMO antenna system (with FSS).

AeroMACS (5.09 GHz – 5.15 GHz), Aeronautical radio location application at (5.43 GHz), 5G NR spectrums ($n77/n78/n79$) and 5G applications.

II. ANTENNA DESIGN AND GEOMETRY

The configuration of the suggested antenna is a 2 elements MIMO antenna using Rogers 4350B substrate with the size of 19 mm × 43 mm. The thickness of the Rogers 4350B substrate is $h = 0.508$ mm, whereas the $\varepsilon r = 3.66$ is used in the proposed antenna design. Furthermore, a periodically arranged FSS array is integrated 10 × 8 Square-shaped structure with Circular Slot (SCS) shaped unit cells (68 elements with surrounding technique) positioned behind the suggested MIMO antenna at a distance of $h_{FSS} = 30$ mm to optimize the performance of the MIMO antenna. The electromagnetic (EM) simulator CST Microwave Studio is used to simulate and model the design. Figure. 1, shows an overview of the stepwise design process, which is discussed in detail in the following sections, along with the optimization techniques used and results obtained.

A. ANTENNA DESIGN

As shown in Figure 2 (a), The MIMO antenna system modelling begins with a single antenna element. The first step involves obtaining an L-shaped radiation monopole patch antenna with inset feed using well-established mathematical equations. [53]. The reflection coefficient results in Figure. 2 (b) show that the L-shaped radiator monopole patch antenna resonates across a wide frequency band from 3.1 GHz to 4.6 GHz. The subsequent step involves incorporating a horizontal slot at the top of the patch antenna, which enhances the impedance matching [53]. This modification results in a bandwidth of 0.2 GHz, with a resonant band from 2.9 GHz to 4.6 GHz as shown in Figure. 2 (b). The last step is adding a slot in the bottom right corner of the antenna's L-shaped radiator side. The final form of the antenna's radiator became chair-shaped, which improved impedance matching and bandwidth from 3.0-6.0 GHz with 3 GHz impedance bandwidth as indicated in Figure. 2 (b). While the antenna underwent three optimization steps resulting in a shift in its frequency bands due to changes in its electrical length, there was an overall improvement in the impedance bandwidth.

Table 1. shows the dimensions of the ultimate single antenna. A 2 elements MIMO antenna fed by a Coplanar Waveguide (CPW) was designed by modifying the single antenna to enhance its radiation characteristics as shown in Figure. 1. The characteristics equations (1)-(7) used to determine the transmission lines width and length to ensure a 50Ω impedance match for the main feed line and a 75Ω impedance match for the second feed line [53], [55].

$$Z_o = \frac{w_{f1}}{h} = \left(\frac{8e^A}{e^{2A} - 2}\right) \tag{1}$$

where,

$$A = \frac{Z_o}{60}\sqrt{\frac{\varepsilon_r + 1}{2}} + \frac{\varepsilon_r - 1}{\varepsilon_r + 1}\left(0.23 + \frac{0.11}{\varepsilon_r}\right) \tag{2}$$

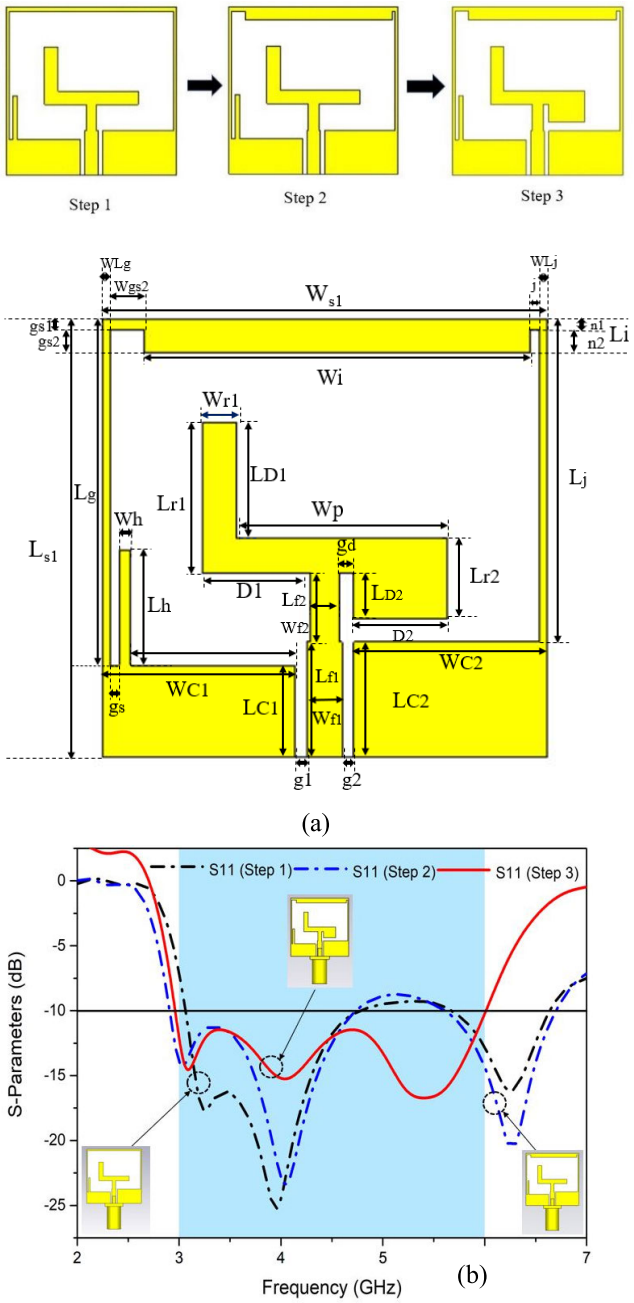

FIGURE 2. (a) The Single element design evolution, (b) The S-parameter curves.

$$l_{f1} + l_{f2} \approx \frac{\lambda_o}{4} \tag{3}$$

$$\lambda_o = \frac{c}{f_o} \tag{4}$$

$$\frac{\Delta L}{h} = 0.412 \frac{\left(\varepsilon_{reff} + 0.3\right)\left(\frac{w_r}{h} + 0.264\right)}{\left(\varepsilon_{reff} - 0.258\right)\left(\frac{w_r}{h} + 0.8\right)} \tag{5}$$

$$\varepsilon_{reff} = \frac{\varepsilon_r + 1}{2} + \frac{\varepsilon_r - 1}{2}\left(\left(1 + 12\frac{h}{w_r}\right)^{-\frac{1}{2}}\right) \tag{6}$$

$$w_r = \frac{v_c}{2f_o}\sqrt{\frac{2}{\varepsilon_r + 1}} \tag{7}$$

TABLE 1. The optimized mimo antenna system elements design parameters (mm).

Parameter.	Value.	Parameter.	Value.	Parameter.	Value
		Parameters of Single Element.			
W_{s1}	19	Lf2	3	Wh	0.5
L_{s1}	19	g1	0.5	Wi	16.5
WC1	8.25	g2	0.5	Li	1.5
Lc1	4	gs	0.4	n1	0.5
WC2	8.25	Lg	15	n2	1
Lc2	5	WLg	0.3	j	0.4
Wf1	1.5	Lj	14	gs1	0.5
Lf1	5	WLj	0.3	gs2	1
Wf2	1.2	Lh	5	Wgs2	1.5
D1	4.65	Wr1	1.5	D2	4
Lr1	6.5	Wp	9	LD2	2
LD1	5	gd	0.65	Lr2	3.5
		Parameters of Two Elements MIMO			
Ws	43	B2	7.91	Lt1	7.5
Ls	19	Wm	5	Lt2	5.5
CWf1	10.75	Ls2	11.5	Wt	4.4
CWf2	10.75	B3	5.58	gi1	0.3
B1	7.91	B4	3.32	gi2	0.3
		Unit Cell Of FSS			
UW	10	Ug	0.1	r3	4.5
UL	10	r1	3.5		
iUL	9.8	r2	4.0		
		FSS Array Parameters			
LFSS	117.50	S	1.5		
WFSS	94.90	h_{FSS}	30		

A transmission line's characteristic impedance is denoted by Z_o, wavelength donated by λ_o, c is the speed of light in free space and f_o is the resonant frequency. The thickness of the substrate is h, ΔL in (5) is the length of the radiator patch where else the effective permittivity is denoted by ε_{reff} in (6). The width of the radiator patch is denoted by w_r, and the dielectric constant is denoted by ε_r in (7), [56]. Equations (1) and (2) were used to determine the feed line width (w_{f1} and w_{f2}) and equations (3) and (4) were used to determine the feed line length (l_{f1} and l_{f2}) of the design with 50 Ω and 75 Ω characteristic impedance (Z_o). The chosen impedance

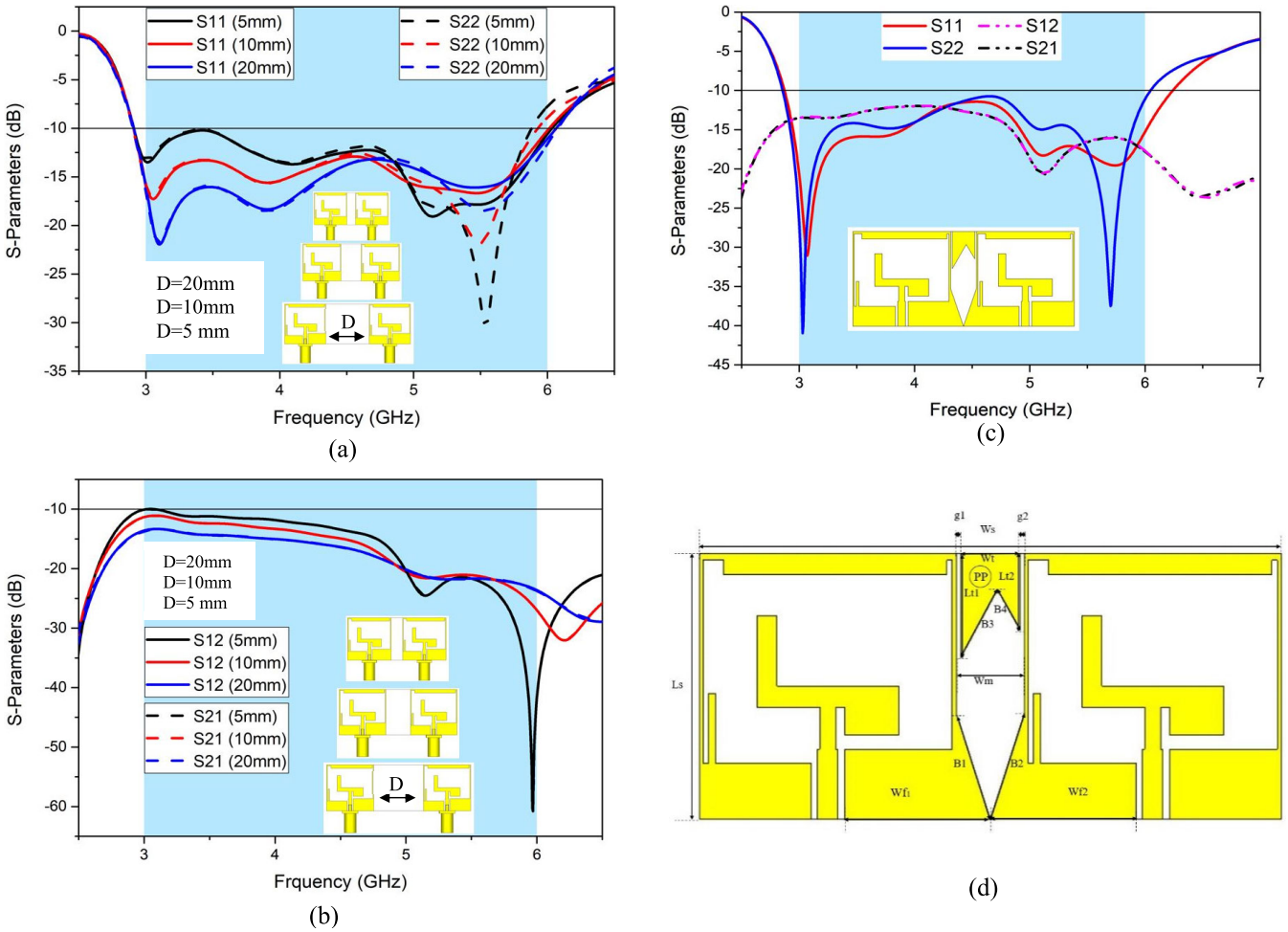

FIGURE 3. MIMO antenna process of reduction of the size, the mutual coupling and enhance the bandwidth, (a) Reflection coefficient (S11, S22), study the spacing between the MIMO antenna elements (20mm,10mm and 5mm), (b) Transmission coefficient (S12, S21), (c) Reflection coefficient (S11, S22) and Transmission coefficient (S12, S21) using Parasitic Element, (d) The proposed MIMO antenna.

of the second feed line is 75 Ω with length l_{f2} and width w_{f2} to enhance the impedance matching at the frequency (3.5 GHz).

Where else equations (5)-(7) are used to determine the length and the width of the radiator patch respectively. The width of the gap Wm between the two components of the MIMO was studied at different dimensions to achieve a compact design and high performance of MIMO. The distance between the MIMO antenna elements studied in different spaces, which are 20mm, 10mm, and 5mm, is equal to 0.3λ, 0.15λ, and 0.075λ, respectively, at 4.5 GHz. The design is advanced to achieve MIMO capability using a decoupling network approach to MIMO. The mutual coupling has been examined using a decoupling network method, as illustrated in Figure. 3.

The decoupling network approach produces good results for wide bandwidth (3-6 GHz) and low mutual coupling at 20mm or 0.3λ at 4.5GHz as the centre frequency. However, the decoupling network technique achieved good results at the expense of the size of MIMO, which becomes 58mm (Ws), as shown in Figure. 3 (a and b). additionally, to reduce the size, a triangular slot with lengths of B1 for antenna one and B2 for antenna two, with a width of 2.5 mm for each of the triangular slots, is integrated into the ground plane of CPW. Figure. 3 (c) and (d) depict these triangular slots form wf1 and wf2 in the MIMO antenna. The design improvement from a single antenna to MIMO enhances the bandwidth, covering the frequency spectrum of 3-6 GHz.

Finally, the parasitic element technique is used to reduce the size and mutual coupling of the proposed MIMO antenna. This type of decoupling approach may be used to minimize the coupling between MIMO antenna elements by implementing a parasitic element between the antennas in a MIMO system and cancelling some of the coupled fields, hence reducing overall coupling on the chosen antenna. These components (parasitic elements or parasitic patches) are not in any way linked to the antennas.

The parasitic element might be anything, such as a resonator or shorted stubs. Parasitic elements can be used as well to enhance the bandwidth, isolation range, and coupling amount and reduce the size of the MIMO antenna [8], [19], [29].

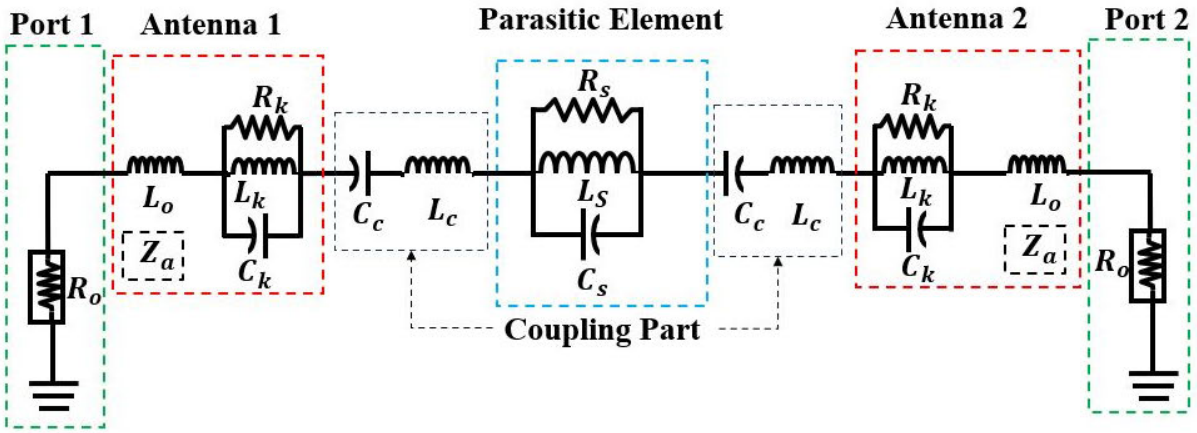

FIGURE 4. Equivalent circuit of the proposed MIMO antenna.

In the proposed MIMO antenna, the parasitic patch (PP) stub with a slot is used to reduce the mutual coupling between the antenna elements. The stub does this by redirecting some of the electromagnetic energy away from the other antenna element. The slot also helps to reduce the mutual coupling by reflecting some of the radiation from the other antenna element, which enhances the isolation. The substrate size of the final Chair-shaped MIMO antenna of two elements is ($19\times43\times0.508$ mm), as illustrated in Figure. 3 (d). Moreover, the Parasitic elements placed on the front side of the substrate between the MIMO antenna elements have reduced the overall size of the Chair-Shaped MIMO antenna by 25.9 % (from 58mm, $0.87\lambda_o$ to 43mm, $0.645\lambda_o$) which reduced the space between the two elements by 75% (from 20mm, $0.3\lambda_o$ to 5mm $0.075\lambda_o$) as shown in Figure. 3 (a)-(c). Hence, The Chair-shaped MIMO antenna has a wider bandwidth than the other MIMO antennas listed in Table 3.

Furthermore, Figure 3(c) shows the simulated reflection coefficients of the MIMO antennas (S11, S22). The reflection coefficients are almost similar, and they resonate in the band from 3 to 6 GHz. This means that the MIMO antenna has a wide bandwidth, which is sufficient for wide bandwidth 5G and sub-6GHz 5G applications. Figure. 3 (c) plots the transmission coefficients for different MIMO antennas, demonstrating significant isolation between the antennas. The minimum transmission coefficient between the antennas is below -10dB within the range of frequency band (3-6 GHz).

B. EQUIVALENT CIRCUIT OF THE PROPOSED MIMO ANTENNA

To visualize the MIMO antenna configuration more clearly, the equivalent circuit of the proposed MIMO antenna is depicted in Figure. 4 [57]. The patch radiators can be modelled through a lumped-element equivalent circuit comprising inductance (L_k), capacitance (C_k) and resistance (R_k). These elements, together, represent the antennas total input impedance (Z_a) across its wideband operating range. The equivalent circuit of the Parasitic Element or Parasitic Patch (PP) isolator is depicted by inductance $L_{s,}$ and the capacitance (C_s) which mainly models the effect of the parasitic element and depends on the length ($L_{t1}+L_{t2}$) and the width (W_t) of the Parasitic element as shown in Figure 3 (d). The losses related to the ohmic, and dielectric properties of the parasitic element's isolator are denoted by the parameters (R_s). The resonance frequency (F_r) of the decoupling structure is dependent on the magnitude of the inductance (L_s), and the capacitance (C_s), is shown by Equation (8). it is worth mentioning that the coupling between the patch and the parasitic element isolator is a combination of inductive (L_c) and Capacitive (C_c) coupling. This coupling is influenced by the gap ($g_1+ g_2$) between the parasitic element isolator and the radiator patch, as illustrated in Figure. 4 [57], [58], [59].

$$f_r = \frac{1}{2\pi\sqrt{L_s C_s}} \tag{8}$$

C. DESIGN OF FREQUENCY-SELECTIVE SURFACE (FSS)

Frequency-selective surfaces (FSSs) are planar structures that are made up of repeating unit cells. (The unit cells can be configured in either one or two dimensions.

The resonance frequency of the FSS is determined by the dimensions, structure, and spacing of the unit cells. Depending on the resonant frequency, angles of frequency, polarization, and dielectric substrate, FSSs can reflect, send, or receive energy from the electromagnetic spectrum. In general, there are two types of FSSs: slot and patch. Slot FSSs function as high-pass filters, while patch FSSs function as low-pass filters [43].

The suggested unit-cell structure of FSS is a square with a circular slot in the centre. Roger 4350B is used as a substrate that is 10 mm × 10 mm in size, 0.508 mm thick, and has a dielectric-constant (ε_r) of 3.66 and a loss tangent ($\tan\delta$) of 0.0017. Figures. 5 (a), (b), and (c) depict the unit cell design. The unit cell was investigated using CST software to design an FSS with a wide bandwidth and a linear reflection phase.

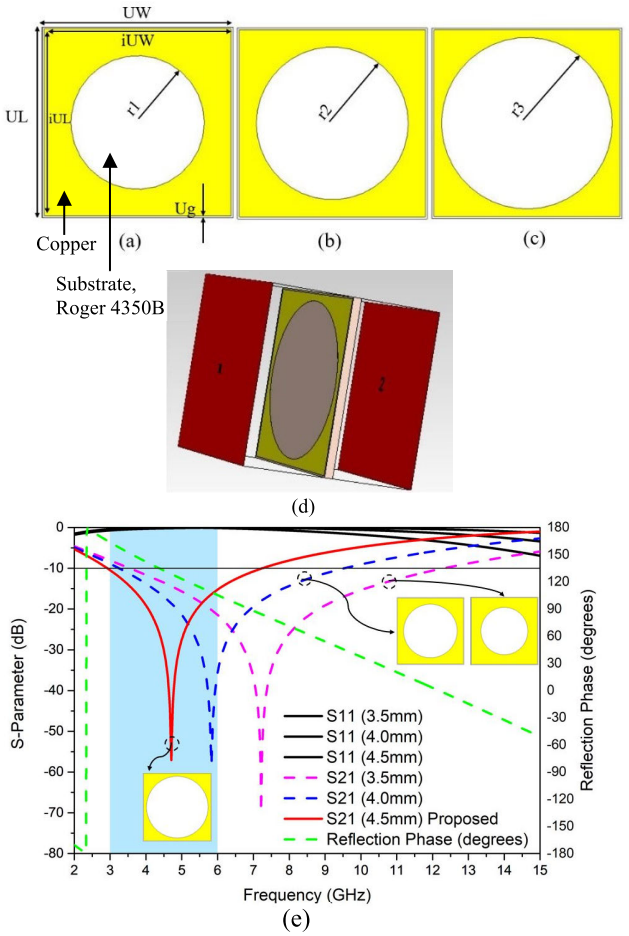

FIGURE 5. (a) and (b); study of unit cell design at different radius (r), (c) The proposed unit cell, (d) Unit cell excitation, (e) S-parameter.

The initial and first design of the proposed new FSS unit cell is based on a conventional squared structure with a circle-shaped slot in the centre. The radius of the circular slot is 3.5 mm. They optimized the design using analytical modelling and simulations to achieve a stopband at 7.21GHz and a bandwidth of 8.77GHz, meaning that it can reflect electromagnetic waves with frequencies between 3.54 GHz and 12.31 GHz. In the second phase, it modified the circular slot to 4.0 mm to create a complementary loop structure (CLS). The CLS unit cell had a stopband at 8.77GHz and a transmission coefficient of −56 dB. However, the response of the CLS unit cell remained insufficient at lower frequencies and attained the intended wide bandwidth stopband. CLS can reflect electromagnetic waves with frequencies between 3.24 GHz and 9.54 GHz.

Finally, to create an optimal circular loop structure (OCLS), increase the radius of the circular slot loop. The OCLS circular slot has a radius of 4.5 mm. The optimized circular slot unit cell (OCLS) achieved a stopband of 4.32 GHz across the entire wideband from (2.92 GHz to 7.24 GHz). The overall size of the CSS, CLS, and OCLS unit cells is the same. The only difference is the radius of the circular slot as shown in Figure. 5 (e). The suggested FSS design, shown in Figure 5 (c), achieves a linearly decreasing reflection phase from 2.92GHz to 7.24GHz. The boundary and symmetry conditions used to simulate the FSS are shown in Figure. 5(d). An FSS's reflection phase is critical for improving the performance of antenna uses. The phase of the FSS must decrease linearly to provide the desired phase reflection to the antenna [36]. Figure. 5(e) shows the FSS's predicted reflection phase as predicted by the simulation.

D. EQUIVALENT CIRCUIT OF THE FSS UNIT CELL (EC)

The design and investigation of the FSS unit cell are shown in Figure. 6(a). An equivalent circuit model of a loop-FSS cell element is used to design the FSS. Figure. 6(b) depicts the equivalent circuit model of a circular loop FSS cell element. The model consists of an inductance (L) and a capacitance (C). The capacitance is due to the circular sectors of the loop, which act as capacitors when transmitting magnetic (TM) mode impact waves impinges on the reflector.

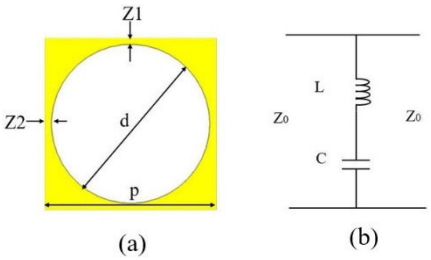

FIGURE 6. (a) The unit cell, (b) predicted the reflection phase and the transmission coefficient (S21), and (c) The Equivalent Circuit (EC).

In contrast to the circular sections, the horizontal or vertical square sections of the loop antenna element act as an inductance (L). Figure 6 illustrates the arrangement of a basic printed loop FSS, featuring both square and circular loops. The dimensions of the FSS cell element, including (p) is the period, (w) is the width, (d) is the side length, and (g) is the inter-element gap, are approximately estimated to be 9 mm, 9.8 mm, 9 mm, and 1.5 mm, respectively. The inductance and capacitance (L and C) in the equivalent printed square or circular loop circuit are connected between the free space impedance (Z0). The values of the inductor (L) and capacitor (C) in an equivalent circuit can be calculated from the reactance (XL) and susceptance (BC) of the circuit. The equations for XL and BC [9], [10], [11], [12], [13], [14], [15], [16], [17], [18] are based on references [42] and [43], respectively.

$$\frac{X_L}{Z_0} = \frac{d}{p} F\,(p, w, \lambda, \theta) \tag{9}$$

$$= \frac{d}{\lambda} cos\theta \left[In \left\{ cosec \left(\frac{\pi w}{2p} \right) \right\} + G(p, w, \lambda, \theta) \right] \tag{10}$$

$$\frac{B_c}{Y_0} = 4\frac{d}{p} F\,(p, g, \lambda, \theta)\, \varepsilon_{eff} \tag{11}$$

$$= 4\frac{d}{\lambda} sec\theta \left[In \left\{ cosec \left(\frac{\pi g}{2p} \right) \right\} + G(p, g, \lambda, \theta) \right] \varepsilon_{eff}. \tag{12}$$

The angle of incidence of the signal is denoted by θ and the wavelength of the signal is denoted by λ. $G\,(p,\, w,\lambda,\, \theta)$ is the correction term determined by the following equation:

$$0.5\frac{1-\beta^2\left[\left(1-\frac{\beta^2}{4}\right)(A_+ + A_-) + 4\beta^2 A_+ A_-\right]}{\left(1-\frac{\beta^2}{4}\right) + \beta^2\left(1+\frac{\beta^2}{2}-\frac{\beta^4}{48}\right)(A_+ + A_-) + 2\beta^6 A_+ A_-} \tag{13}$$

where A_+ and β are

$$A_\pm = \frac{1}{\sqrt{\left[1 \pm \frac{2p\sin\theta}{\lambda} - \left(\frac{p\cos\theta}{\lambda}\right)^2\right]}} - 1 \tag{14}$$

And

$$\beta = \sin\left(\frac{\pi w}{2p}\right) \tag{15}$$

The impedance (Z1) of the horizontal or vertical sections of the FSS cell element is used to calculate the (L and C) for transverse electric (TE) mode wave incidence. The impedance (Z2) of the circular sections utilized for (TM) mode impact waves. The presence of a circular loop ((πd)) compared to a square loop *(4d)* results in a $\pi/4$ factor that affects the environment. Additionally, the non-continuous nature of the conductor reduces reactance by d/p. ($\pi d/2$) is the length of the half-circular loop which introduces a factor of $\pi/2$ compared to (d) which is the straight-line of the square loop. ε_{eff} represents the effective permittivity of the substrate. Equations (16) and (17) provide adapted expressions for circular loop (XL) and (BC), which are then used to calculate the lumped inductance (L) and capacitance (C).

$$\frac{X_L}{Z_0} = \frac{\pi}{4}\frac{d}{p}F\,(p,\, w,\, \lambda,\, \theta) \tag{16}$$

$$\frac{B_c}{Z_0} = \frac{\pi}{2}4\frac{d}{p}F\,(p,\, g_a,\, \lambda,\, \theta)\,\varepsilon_{eff} \tag{17}$$

In (18), the average gap between the circular elements is denoted by (ga).

$$g_{a=\rho-\frac{\pi d}{4}} \tag{18}$$

E. METALIC FSS ARRAY REFLECTOR

The proposed MIMO antennas exhibit degraded performance due to coupling between the two antennas. For the enhancement of the bandwidth, the gain, and the isolation of the antennas, an FSS can be used. An FSS is a periodic arrangement of small structures that can control the reflection and transmission of electromagnetic waves.

The proposed unit cell is designed to operate at 3-6 GHz. It's printed using Rogers 4350B substrate that is 0.508 mm thick. The unit cell is simulated using CST in the time domain. As shown in Figure. 5 (c), the final optimized unit cell configuration is a square patch with a circular loop geometrical pattern in the centre. The boundary conditions and the port assignments employed for stimulating the unit cell are shown in Figure. 5 (d). The unit cell's reflection coefficient curve in Figure. 5 (e) demonstrates that it is resonant at 4.7 GHz (2.92 - 7.24 GHz). Additionally, the plot of the transmission coefficient shows that the FSS unit cell demonstrates minimal loss (nearly zero) at the resonant frequency. This means that nearly all of the electromagnetic waves within the desired frequency band are transmitted through the unit cell as depicted in Figure. 5 (e).

To design an FSS surface that meets the requirements of antenna applications, the FSS surface should be able to cover the bandwidth as the suggested MIMO antenna. In the case of a wideband antenna operating from 3.0 to 6 GHz, both the antenna and the FSS should have this frequency range. The MIMO antenna in this study is integrated with a wide stopband FSS, as shown in Figure 1 (d). The FSS surface needs to be placed a half-wavelength $\lambda/2$ away from the antenna to minimize the coupling between the two (the antenna and the FSS surface). When the FSS surface is placed at $\lambda/2$ from the antenna, the reflected wave will combine with the incident wave in phase, which means that the two waves will add together to create a stronger signal. This results in improved radiation gain, which is the ability of the antenna to direct its energy in a specific direction.

The total propagation distance between the FSS and the antenna is represented by ϕs, which includes the phases of the antenna's transmitted denoted by ϕt and reflected waves denoted by ϕr. This means that the phase of the reflected wave will depend on the distance between the FSS surface and the antenna.

$$\emptyset t = \emptyset r + \emptyset s \tag{19}$$

$$\emptyset s = 2 \times 2\pi f \times \frac{g}{c} \tag{20}$$

The speed of light (c), the gap between the antenna and the metallic reflector (g), and the phase of the transmitted wave (ϕt). The phase of the transmitted wave can be either 0 or an integral multiple of 2π [45].

The proposed FSS is placed behind the radiating element to reflect the return radiation from the antenna. This arrangement allows the FSS to adjust the phase of the return radiation, thereby enhancing the antenna gain. The distance between the reference antenna and the FSS surface is calculated using the equation below [45].

$$\emptyset_{FSS} - 2\beta h_{FSS} = 2n\pi$$
$$when\ n = \ldots -2, -1.0.1.2, \ldots \tag{21}$$

The phase of the reflected wave from the FSS layer is denoted by π. The gap between the antenna and the FSS layer is denoted by h_{FSS}. The open space propagation wave constant is denoted by β. The open space propagation wave between the reflected wave from the FSS layer and the antenna is represented by ($\lambda/2$).

Taking the centre frequency 4.5 GHz and ϕfss $= 0$, for example, h_{FSS} is calculated as 33.33 mm and $h_{FSS} = 30$ mm is chosen here. The spacing between the FSS layer and the MIMO antenna is adjusted to maximize the MIMO antenna's

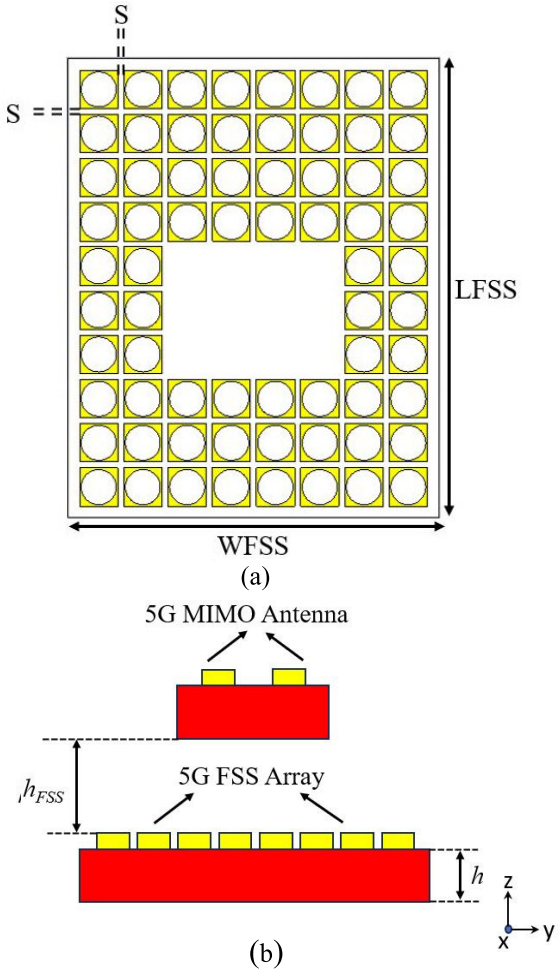

FIGURE 7. (a) 68 elements of FSS array with surrounding technique (b) Side view of 2×2 MIMO antenna with FSS.

gain across the entire frequency band because the FSS is wideband.

The proposed work specifies $h_{FSS} = 30$ mm as the distance between the FSS layer and the MIMO antenna. Additionally, an FSS array is created by arranging 10 × 8 unit cells periodically in a space of S. The FSS array layer dimensions are *WFSS*× *LFSS*. To improve the antenna performance, the FSS array is positioned behind the MIMO antenna at a distance of h_{FSS}, as shown in Figure. 7 (a) and (b) respectively. As demonstrated in Figure. 8, the addition of FSS (Full Cells of FSS array) improves the performance of the MIMO antenna only somewhat. The bandwidth of the proposed MIMO antenna affects the reflection coefficient, which shifts to a lower frequency range of (2.85 GHz - 5.95 GHz) with a maximum gain from 3.63 dBi to 7.33 dBi. This scenario requires a novel technique to enhance the MIMO gain while maintaining the other performance characteristics of the MIMO antenna.

A novel approach was employed to enhance the MIMO antenna gain without impacting the performance of other MIMO antenna characteristics and without increasing the size of the FSS array. The FSS arrays surrounding the

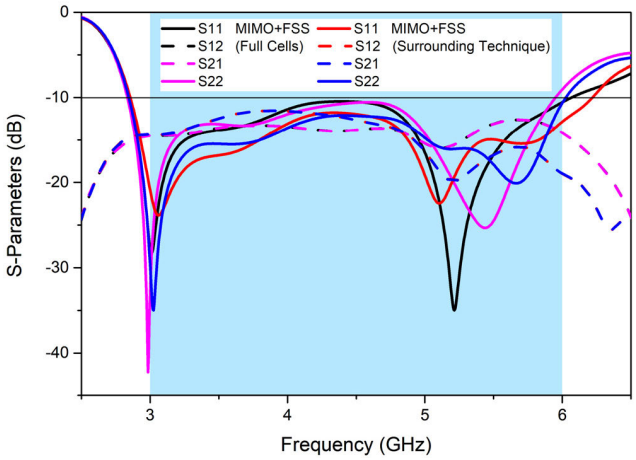

FIGURE 8. The reflection coefficient and the transmission coefficient of the MIMO antenna system with FSS array (full cells) and the FSS array (surrounding technique).

technique improve the MIMO antenna gain from 3.63 to 7.97 dBi. which is increased by 4.34 dBi while maintaining bandwidth from (3-6 GHz). The surrounding technique eliminates certain parts (some cells) of the FSS array behind the suggested MIMO antenna to enhance the MIMO antenna's performance in terms of gain without impacting other antenna characteristics. After applying the surrounding technique, the FSS array of 10 × 8 unit cells becomes 64 unit cells. Additionally, the bandwidth of the MIMO antenna was also improved by using the Surrounding technique. Figure. 8 shows the reflection and the transmission coefficients of the suggested MIMO antenna system using full cells and the surrounding technique. Moreover, the surrounding technique enhances the suggested MIMO antenna system's gain, bandwidth, and isolation without increasing the FSS array's size. The distance between the MIMO antenna and the FSS array using the surrounding technique was investigated at different distances, 20 mm, 25 mm, and 30 mm, as illustrated in Figure. 9. The plot of the reflection and transmission coefficients is depicted in Figure. 10 illustrates the enhancement in impedance bandwidth achieved by employing FSS with the MIMO antennas.

The impedance bandwidth is improved to encompass the frequency range of (3-6 GHz). Moreover, the curves of the transmission coefficient in Figure 10 indicate the minimum isolation between the two Antennas without FSS is approximately −11.55 dB, which further improves to −12 dB after applying the FSS array across the entire operational frequency band.

The MIMO antennas exhibit maximum isolation between Antenna 1 and Antenna 2, reaching approximately −21 dB without the FSS array and −20 dB with the FSS array. Furthermore, the suggested MMIMO antenna has a minimum reflection coefficient without the FSS array achieved is −10.7 dB, and it's enhanced to −12 dB with the FSS array. The maximum reflection coefficient between Antenna 1 and Antenna 2, reaches approximately −41 dB without the FSS

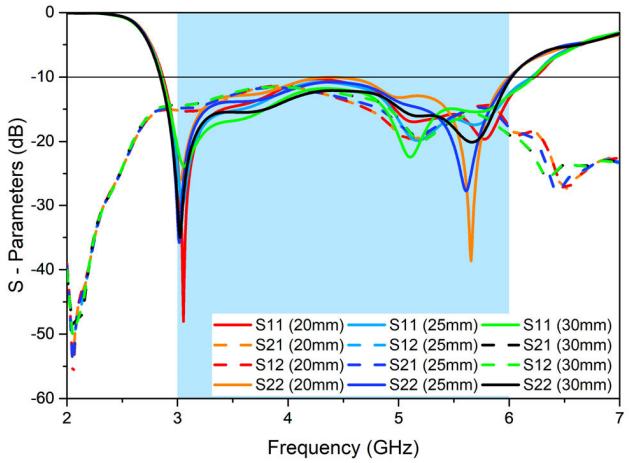

FIGURE 9. The distance investigation between the proposed MIMO antenna and the FSS array (surrounding technique).

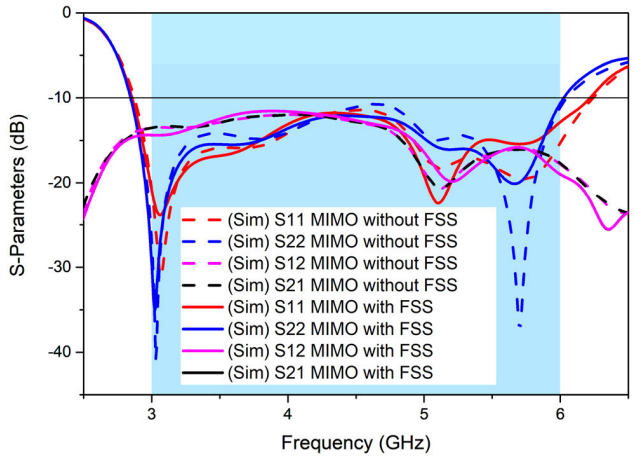

FIGURE 10. MIMO antenna system with and without FSS array (surrounding technique).

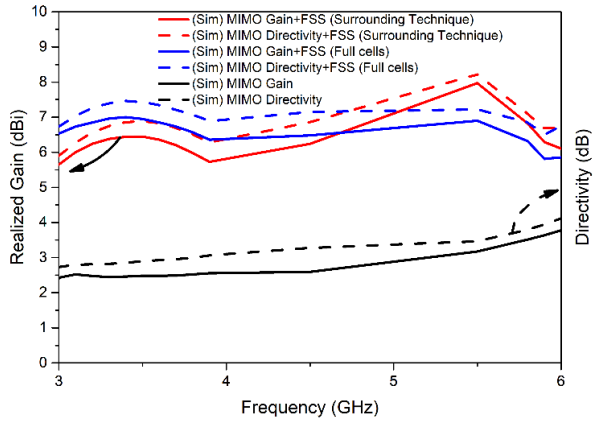

FIGURE 11. Gain and Directivity of MIMO without FSS array, MIMO with FSS array (Surrounding Technique) and MIMO with FSS array (Full Cells).

array. With the FSS array, the maximum reflection coefficient is −38 dB. Figure. 10 displays the transmission coefficient and reflection coefficient curves, illustrating the minimum and maximum values for the MIMO antenna, both with and without the FSS array.

The performance of the suggested MIMO antenna across the entire operational frequency band is significantly enhanced by the FSS. Figure. 11 compares the simulated gain and directivity of the proposed MIMO at various stages of design and different operating frequencies (3-6 GHz). The results show that adding an FSS array to the antenna at the first step increases the gain and directivity.

In addition, the peak gain of the proposed Chair-Shaped compact MIMO antenna achieved is 3.63 dBi at (6 GHz).

Furthermore, by implementing the FSS array with (full cells), the gain of the MIMO antenna increased by approximately 3.3 dBi. As a result, the simulated peak gain achieved is 7 dBi at (3.4 GHz). However, the bandwidth of the MIMO antenna system is impacted by this enhancement. Using the surrounding technique on the FSS array enhanced the gain and bandwidth of the MIMO antenna system. The peak simulated gain is 7.97 dBi at 5.5 GHz, which is an increase of 4.34 dBi over the MIMO antenna system without the FSS array as illustrated in Figure. 11.

F. SURFACE CURRENT DISTRIBUTION

The proposed MIMO antenna has reduced mutual coupling because the currents on the surfaces of the antennas flow in opposite directions. This can be seen in Figure 12, which shows the surface current distribution. (Mutual coupling is increased when the currents on the adjacent sides of two antennas flow in the same direction. The mutual coupling is reduced when the currents flow in opposite directions [54]. The parasitic element in the proposed MIMO antenna is designed to create a surface current that cancels out (or flows in the opposite direction to the current) the current on the right arm of the first antenna as shown in Figure. 13. Thus, the mutual coupling between the two antennas is minimized.

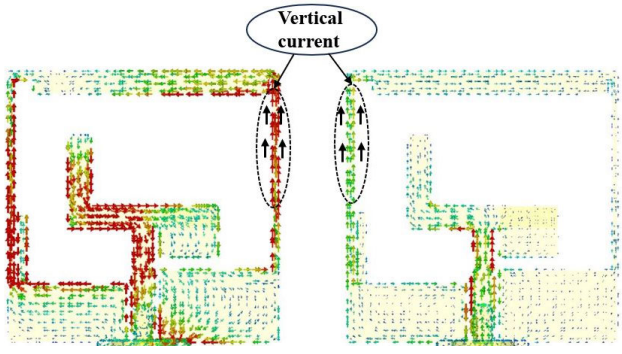

FIGURE 12. Surface currents distribution at 3.6 GHz of Proposed MIMO antenna without parasitic elements technique when port-1 is excited.

Figure 14 shows the electric current flows on port 1 of the proposed MIMO antenna at 5.8 GHz with two different techniques: FSS (a) using a full cell, and (b) using a surrounding technique. These simulations were conducted with the termination of the other port using 50Ω

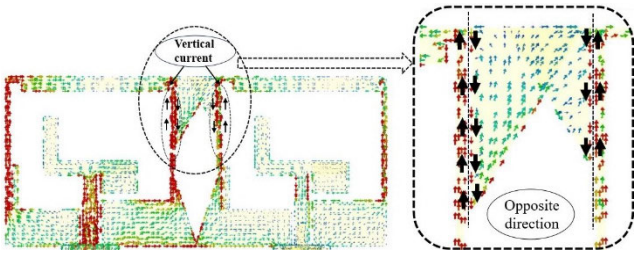

FIGURE 13. Surface currents distribution at 3.6 GHz of proposed MIMO antenna with parasitic elements technique when port-1 is excited.

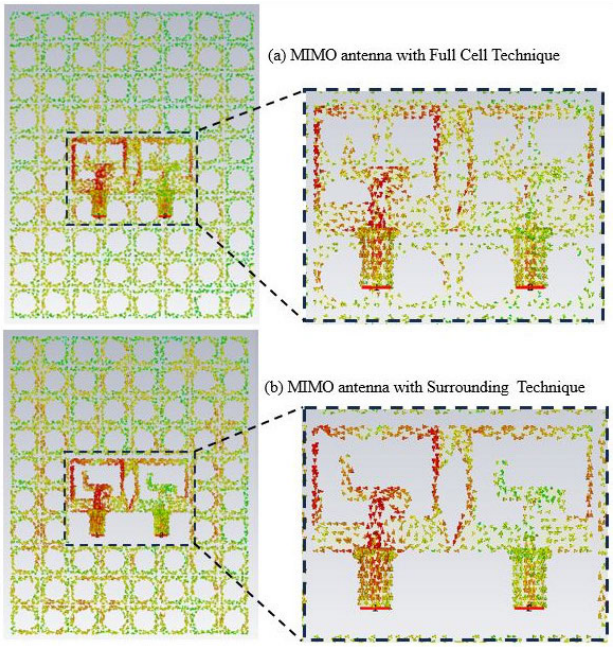

FIGURE 14. Surface current distribution at 5.8 GHz of proposed MIMO antenna with (a) Full Cell Technique and (b) Surrounding Technique.

loads. The FSS-loaded MIMO antenna is more efficient at radiating energy because the surface current on the antenna is redistributed and some of the energy from the radiating patch is coupled to the surface of the FSS.

The surrounding technique FSS array redistributes the surface current on the right-side patch of the MIMO antenna more efficiently, which leads to a more coherent superposition of energy in the far field. This enhances the gain of the MIMO antenna compared to the full cells FSS array. The gain enhancement is a result of both the increased aperture efficiency and the coherent superposition of energy from the MIMO antenna patch and the FSS cells in the far field [35], [37].

III. EXPERIMENTAL RESULTS

To experimentally validate the proposed MIMO antenna with FSS, a fabrication process is carried out as shown in Figure. 15 (a) and (b). Roha cell spacers are utilized to stack the FSS above the antennas. The following sections present a comparative analysis between the simulated and measured results.

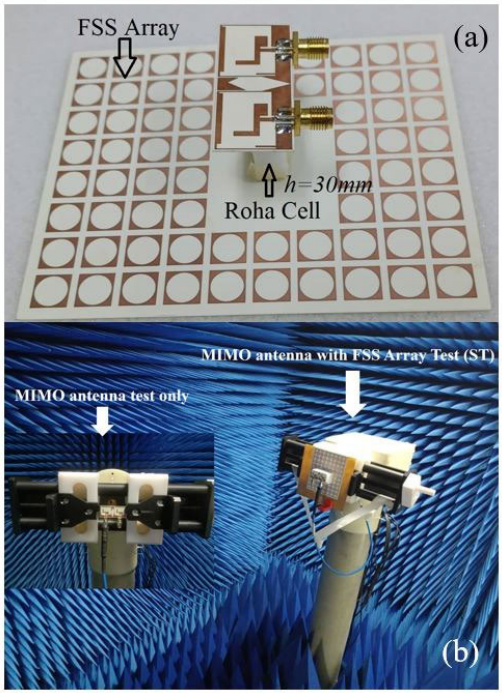

FIGURE 15. (a) Fabricated MIMO antenna system (MIMO and FSS Array), (b) Far-field measurement setup.

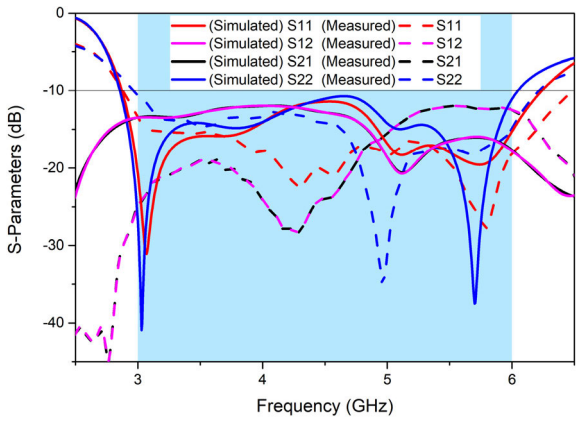

FIGURE 16. Measured and simulated S-Parameter results of the MIMO antenna without FSS array surrounding technique (ST).

A. REFLECTION COEFFICIENT AND ISOLATION

The S-parameters of the proposed MIMO antenna with and without the FSS array are measured using a Vector Network Analyzer (VNA). The simulated and measured S-parameters results of the MIMO antenna without and with the FSS array are shown in Figures. 16 and 17 respectively. The parameters S11 and S22 represent the reflection coefficients of the two antenna elements, while the S12 and S21 parameters represent the isolation between the two elements.

Figure. 16 shows the results of measuring the reflection coefficient of the proposed MIMO antenna without the FSS array. The results show that the frequency band of the MIMO antenna is resonating in (3-6 GHz) with a 10 dB impedance bandwidth of (3 GHz). Figure. 17 shows that the MIMO

antenna with the FSS Array using Surrounding Technique (ST) has similar characteristics to the MIMO antenna without the FSS Array. It operates at (3-6 GHz) with an impedance bandwidth of (3 GHz). The proposed MIMO antenna system matched well between the measured and simulated results with only minor discrepancies due to fabrication flaws and cable losses.

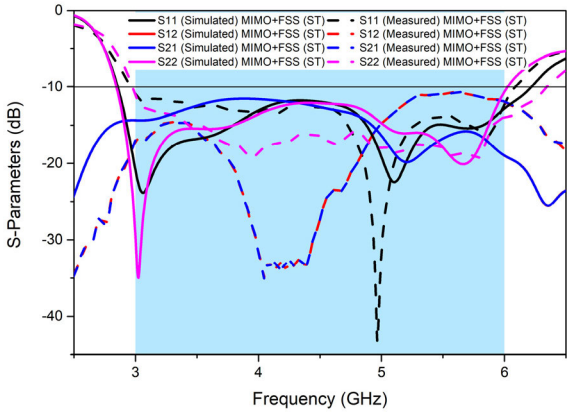

FIGURE 17. Measured and simulated S-parameter results of the MIMO antenna with the FSS array surrounding technique (ST).

B. RADIATION PATTERN AND GAIN

In an anechoic chamber at the University Technical Malaysia Melaka (UTeM), Malaysia, the radiation patterns of the proposed MIMO antenna with and without an FSS array were measured. The transmitter was a standard gain horn antenna, and the receiver was the proposed antenna. To obtain measurements at different orientations, the proposed MIMO antenna with and without the FSS array was rotated 360 degrees. The far-field radiation patterns of Antennas 1 and 2 for two different cut planes: the XZ-plane ($\emptyset = 0°$) and the YZ-plane ($\emptyset = 90°$). Figure. 20 (a), (b), and (c) depict the radiation patterns of Antenna1 and Antenna2 at three different frequencies, (3.1 GHz), (3.5 GHz), and (5.8 GHz) for both the XZ and YZ phases. The measured Cross-Polarization radiation of the proposed MIMO antenna system with and without FSS shown in Figure 20.

The proposed MIMO antenna system radiation patterns are almost equally well in all directions according to the simulated and measured results. This is because the antenna has quasi-omnidirectional radiation patterns in both the XZ and YZ planes. However, the radiation patterns exhibit slight distortion in the measured results due to the non-planar configuration of the antenna and fabrication imperfections. The curves of the measured realized gain and directivity of the suggested MIMO antenna system with and without an FSS array at different frequencies are shown in Figure. 18. The measured realized gain of Antenna1 with the FSS array is 7.96 dB at (5.3GHz), and Antenna2 with the FSS array has 7.89dB of realized gain at (5GHz). These measured results agree with the simulated results.

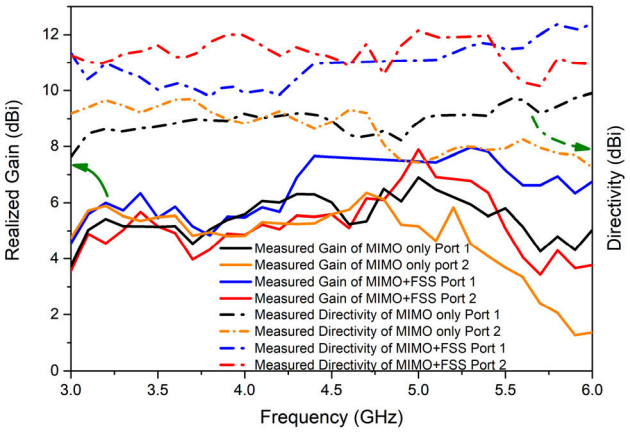

FIGURE 18. Measured of realized gain and directivity of port 1 and port 2 with and without the FSS array of the MIMO antenna system.

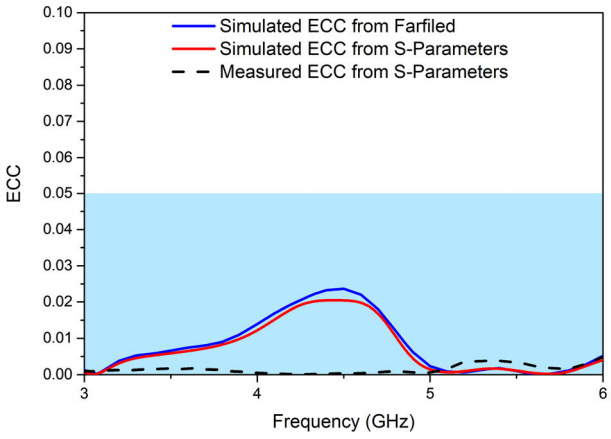

FIGURE 19. The measured ECC and simulated from both, S-Parameters, and far-field patterns.

IV. MIMO PERFORMANCE

ECC, DG, MEG, CCL, and TARC are all important parameters to consider when evaluating the performance of a MIMO antenna. These parameters will be discussed further in the subsections that follow for the suggested MIMO antenna design.

A. ENVELOPE CORRELATION COEFFICIENT (ECC)

ECC is a measure of how closely two MIMO antenna radiation patterns are correlated. The ECC for two perfectly independent antennas would be zero [46]. In practice, ECC values below 0.05 are considered acceptable. The ECC of the MIMO antenna can be calculated using both its S-parameters and its far-field radiation patterns. Equations (22) and (23), respectively, are used to calculate the ECC from the S-parameters and far-field. Calculating the ECC from the far-field radiation patterns using equation (23) is more accurate.

The ECC was calculated from the far-field of the MIMO antenna using equation (23) as recommended by [46].

$$ECC = \frac{|Sii * Sij + Sji * Sjj|^2}{\left(1 - |Sii|^2 - Sij^2\right)\left(1 - |Sji|^2 - Sjj^2\right)} \quad (22)$$

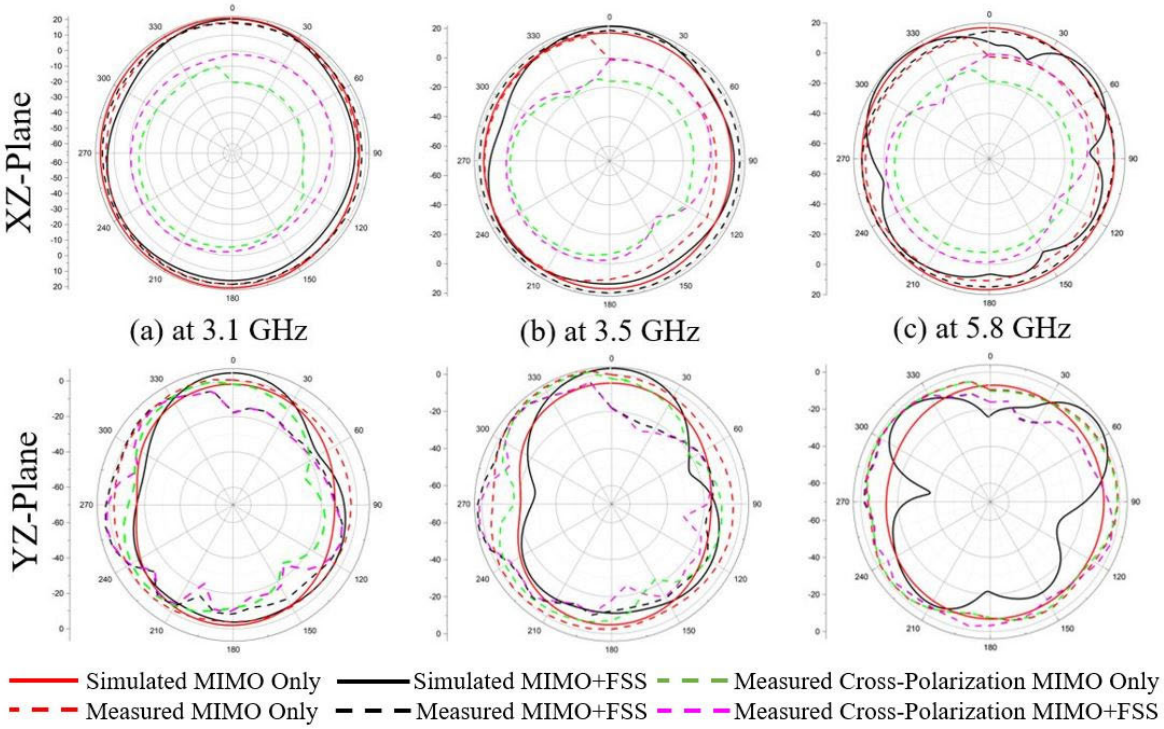

FIGURE 20. Simulated and Measured Cross-Polarization, XZ antenna (1) and YZ antenna (2) Radiation pattern of MIMO antenna system with and without FSS at different frequencies, (a) 3.1 GHz, (b) 3.5 GHz and (c) 5.8 GHz.

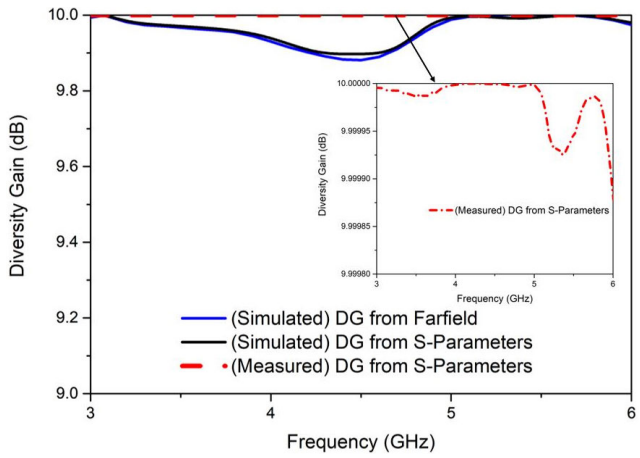

FIGURE 21. The measured DG and simulated from both, S-Parameters, and far-field patterns.

$$ECC = \frac{\left|\iint \left[\vec{R}i\,(\theta,\varphi) \times \vec{R}j\,(\theta,\varphi)\right] d\Omega\right|}{\iint \left|\vec{R}i\,(\theta,\varphi)\right|^2 d\Omega \iint \left|\vec{R}j\,(\theta,\varphi)\right|^2 d\Omega} \tag{23}$$

where Ω is the solid angle, $\vec{R}i\,(\theta,\varphi)$ and $\vec{R}j\,(\theta,\varphi)$ are the radiation patterns of the i^{th} and j^{th} antenna, respectively.

Figure. 19 depicts the proposed MIMO antenna's ECC curves calculated using both equations (22) and (23). Both methods calculate ECC values that are very similar and well below 0.020 (from the S-Parameters) and 0.023 (from far-field) respectively. The investigation of the ECC of the proposed MIMO antenna has shown that it has achieved very high port isolation (low ECC) and excellent diversity performance, as evidenced by the measured ECC value of 0.004, which is well below the ECC acceptable value of 0.05.

B. DIVERSITY GAIN (DG)

DG is the reduction in transmitted power required to achieve a certain level of performance in a MIMO system when diversity is used. Equation (24) is used to calculate the DG.

$$DG = 10\sqrt{1 - |ECC|^2} \tag{24}$$

Figure. 21 depicts the DG of the suggested MIMO antenna, calculated using both the S-Parameters and the Far-field patterns. The simulated and measured DG values remain consistently greater than 9.99 dB across the frequency bands of interest. This closeness to the DG ideal value of 10 dB indicates that the suggested MIMO antenna exhibits excellent diversity performance.

C. CHANNEL CAPACITY LOSS (CCL)

MIMO antenna can transmit multiple data streams simultaneously, which typically increases channel capacity. However, the correlation between the antenna elements can reduce the channel capacity. CCL is a metric that measures how much channel capacity is lost due to correlation. CCL can

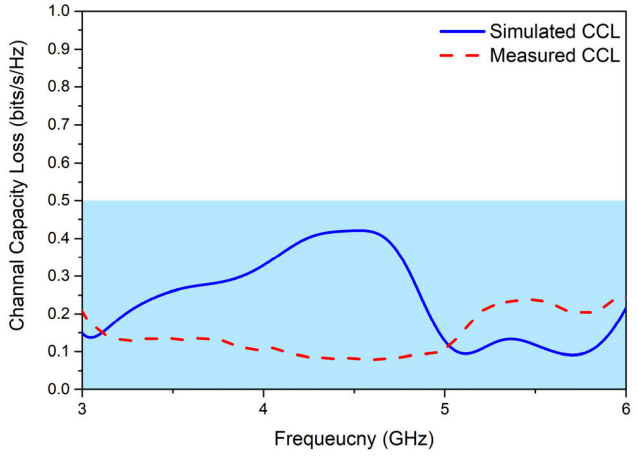

FIGURE 22. The measured and simulated of the CCL.

be calculated using the equations below (25)-(30).

$$C_{loss} = -\log_2 det\left(\Psi^R\right) \tag{25}$$

where ΨR is the matrix that describes the correlation between the elements of the receiving antenna. It can mathematically be defined as follows.

$$\Psi^R = \begin{bmatrix} \Psi_{ii} & \Psi_{ij} \\ \Psi_{ji} & \Psi_{jj} \end{bmatrix} \tag{26}$$

where,

$$\Psi_{ii} = 1 - \left(|S_{ii}|^2 + |S_{ij}|^2\right) \tag{27}$$

$$\Psi_{jj} = 1 - \left(|S_{jj}|^2 + |S_{ji}|^2\right) \tag{28}$$

$$\Psi_{ij} = -\left(S_{ii}^* S_{ij} + S_{ji}^* S_{jj}\right) \tag{29}$$

$$\Psi_{ji} = -\left(S_{jj}^* S_{ji} + S_{ij}^* S_{ii}\right) \tag{30}$$

Figure. 22 shows the value of the CCL of the suggested MIMO antenna as calculated using the above CCL equations. Across the frequency band of interest, the simulated and lab environment-measured values of CCL are less than (0.45 and 0.2 bit/s/Hz) respectively. This is below the industry limit of (< 0.5 bits/S/Hz) [35], [46], indicating that the suggested MIMO antenna performs well in terms of channel capacity.

D. MEAN EFFECTIVE GAIN (MEG)

MEG is a measure of how well a MIMO antenna can collect and concentrate power in a complex environment with multiple signal reflections. Equation (31) is a specific formula for calculating MEG in a MIMO antenna, considering the number of antennas and the characteristics of the environment.

$$MEG_i = 0.5\mu_{irad} = 0.5\left(1 - \sum_{j=1}^{K} |S_{ij}|^2\right) \tag{31}$$

where the MEG of a MIMO antenna depends on (K) the number of antennas, (i) is the active antenna and ($\eta irad$) is the radiation efficiency of the (ith) antenna. The simulated values of MEG for Antenna1 and Antenna2 were calculated

TABLE 2. Simulated of MEG of the proposed MIMO antenna.

Frequency (GHz)	MEG 1 ($-dB$)	MEG 2 ($-dB$)	Ratio of MEG MEG1/MEG2 (dB)
3	6.4929	6.4352	1.0089
3.5	6.7192	6.8305	0.9837
4.0	6.9563	6.9569	0.9999
4.5	7.1680	7.2309	0.9913
5.0	6.3226	6.4806	0.9756
5.5	6.3568	6.3773	0.9967
6.0	6.4325	6.8850	0.9342

using the expanded equations (32) and (33) and are shown in Table 2.

$$MEG_1 = 0.5\mu_{irad} = 0.5\left(1 - |S_{11}|^2 - |S_{12}|^2\right) \tag{32}$$

$$MEG_2 = 0.5\mu_{irad} = 0.5\left(1 - |S_{21}|^2 - |S_{22}|^2\right) \tag{33}$$

The MEG should be between two standard values for good diversity performance.

$$-3 \leq \text{MEG (dB)} < -12.$$

Respectively, Table 2 and Figure. 23 shows that the simulated and measured MEG values of the suggested MIMO antenna are all within acceptable range. The MEG value measured in the lab environment is (−3.13 dBi), which is within the acceptable range. This indicates that the suggested MIMO antenna performs well in multipath fading environments. The results show that the suggested MIMO antenna is within MEG's standard range of (−3dB) to(−12dB). The *MEG*1 to *MEG*2 *ratio* is also *one*, indicating good diversity performance.

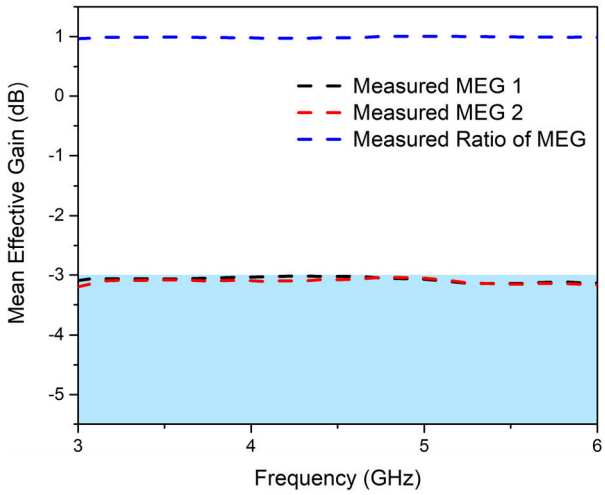

FIGURE 23. Measured Mean Effective Gain (MEG) and ratio of MIMO antenna.

E. TOTAL ACTIVE REFLECTION COEFFICIENT (TARC)

TARC is an important metric for evaluating the performance of MIMO antennas. TARC is the ratio of the reflected power

TABLE 3. Comparison with related work.

References	No. of ports	Optimization Techniques.	MIMO Dimensions (W×L×h) mm^3, Overall Dimensions mm, Material.	Frequency (GHz)	Gain (dBi)	Efficiency (%)	Isolation ($-dB$)	ECC	TARC (dB)	CCL ($bits/S/Hz$)
[47]	2	MIMO+SIW +SSPP	60×120×0.8, 60×120×1, F4B	6.4, 8.2	-	90.9-86.7	20	-	-	-
[48]	2	MIMO+ Metallic	220×150×100, FR4	0.7-1,1.7-3, 3.3-3.8	5.5-8	-	17	-	-	-
[35]	2	MIMO+FSS	50 × 70 × 1.6, 50 × 70 × 9.5, FR-4	2.4, 2.95, 3.2, 3.6, 5.5	3-4	55-65	< 30	<0.25	<-8	<0.3
[2]	4	MIMO+FSS	112 × 112 × 1.6, 112 × 112 × 30, FR4	5.15-5.35	4.9, 7.2	81-89	22	0.11	-	-
[38]	2	MIMO+SRR + EBG	150×85×1.57, RT 5880	5.11-5.25	7.0	95	> 27	< 0.06	-	-
[49]	2	MIMO+PIN Diode+ DC biasing circuit	120×60×1.575, FR4	0.81-1, 3.5-5.3, 1.8-2.2, 4.3-4.8	1.06,1.23 ,2.37, 2.97,1.5 ,1.87	46.3-74.5 55.2-65	>13	0.26 0.08	-	-
[50]	2	MIMO + Closed loop	120×70× 8.15, Taconic	4.7-5.1	3.5	93	28	< 0.05	-	-
[51]	4	MIMO+ metal wall	42 × 42 × 0.4, 100 × 100 × 10, FR4	3.3-5	6.1-7.5	>80	15	< 0.03	<-10	-
[52]	2	MIMO+ Metasurface	29 × 23 × 1 79.5 × 79.5 × 10, FR4	6.75 - 14.5	8.8	72	15	0.005	-10	0.35
Proposed	2	MIMO+FSS	19 × 43 × 0.508, 117.5 × 94.9 × 30, RO4350B	3-6	7.96	97	>13	0.004	<-8	0.2

from the MIMO antenna to the transmitted power into the MIMO antenna. A low TARC value indicates that the MIMO antenna performs well in terms of transmitting power while minimizing reflection.

The square root of the total incident power divided by the MIMO antenna's radiated power in equation (34) used to calculate the TARC of the MIMO antenna.

$$\Gamma_a^t = \Gamma = \frac{\sqrt{\left(\left|S_{11} + S_{12}^{e^{j\theta}}\right|^2\right) + \left(\left|S_{21} + S_{22}^{e^{j\theta}}\right|^2\right)}}{\sqrt{2}} \quad (34)$$

The antenna was connected to an ideal phase shifter and the phase angle (θ) was varied from (0° to 180°) in (30°) steps to analyze the TARC of the proposed MIMO antenna. Figure. 24 depicts the simulated and measured TARC values. Equation (34), [35] is used to calculate the TARC Values, which considers the reflection coefficients (S11 and S22) of the two antenna ports, the port isolation S12 and S21), and the phase angle (θ). The TARC values are all below (<0dB) across the bands of interest, which means that the suggested MIMO antenna has good port isolation and can radiate power efficiently.

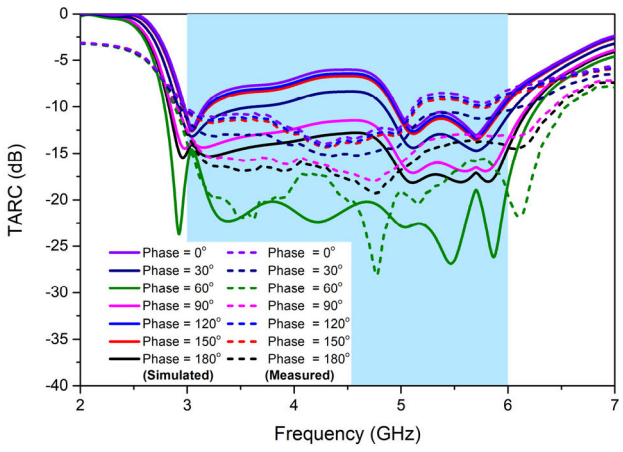

FIGURE 24. The simulated and measured TARC (dB) curves of the MIMO antenna.

F. COMPARISON WITH THE RELATED WORK

The proposed Sub-6GHz 5G MIMO antenna system is designed for a variety of wireless applications and is a significant improvement compared to other recent state-of-the-art designs in Table 3. The proposed antenna is highly competitive in terms of size, profile, efficiency, and band coverage. The proposed MIMO antenna uses parasitic elements to reduce its size by 25.9 % and cover the frequency band of 3-6 GHz. The suggested MIMO antenna gains with an FSS array are also significantly higher than other reported designs [2], [35], [38], [47], [48], [49], [50], [51]. The

suggested MIMO antenna has good values for ECC, CCL, and TARC, which are important performance metrics for MIMO antennas. Most of the other antennas in Table 3 are not evaluated for CCL and TARC. The proposed MIMO antenna system is a highly advantageous choice for both current and future communication devices and technologies due to its excellent performance.

V. CONCLUSION

A two-element MIMO antenna using a single-layered FSS is presented, supporting Sub-6GHz 5G applications. (1 × 2) MIMO antenna using coplanar waveguide (CPW) fed, Moreover, the proposed compact Chair-Shaped MIMO antenna size is 19×43 × 0.508 mm ($0.285\lambda_o \times 0.645\lambda_o \times 0.007\lambda_o$). The parasitic element technique is used to reduce the size of the suggested MIMO antenna by 25.9% and to enhance the mutual coupling. The suggested MIMO antenna system has a measured impedance bandwidth of 3 GHz, covering the frequency range (3 GHz – 6 GHz), with a radiation efficiency of 97%. Moreover, a novel technique (Surrounding technique) was used on the FSS array to enhance the MIMO antenna gain and isolation without impacting the performance of other MIMO antenna characteristics and without increasing the size of the FSS array. The placement of the FSS array (h_{FSS}) at 30 $mm(0.45\lambda_o)$ behind the proposed MIMO antenna enhances the isolation and the gain of the system by approximately 4.34 dBi. The measurements indicate a peak gain of 7.89 dB. In addition, the proposed MIMO antenna system has an excellent performance in all other measured metrics, including radiation pattern, ECC, CCL, TARC and MEG.

This makes the suggested MIMO antenna system a strong contender for use in Sub-6GHz 5G band (3-6GHz) and supporting various other wireless communication systems like Wearable antenna at (4.4-5 GHz), AeroMACS at (5.09–5.15 GHz), Aeronautical radio location application at (5.43 GHz), an Unmanned aerial vehicle (UAV) at (5.7-5.8 GHz), Cardiac pace marker at (5.8GHz), 5G new radio (NR) spectrums such as n77/n78/n79 and 5*G* applications.

REFERENCES

[1] Q. Zhou and H. Dai, "Joint antenna selection and link adaptation for MIMO systems," *IEEE Trans. Veh. Technol.*, vol. 55, no. 1, pp. 243–255, Jan. 2006, doi: 10.1109/TVT.2005.861211.

[2] G. Das, N. K. Sahu, A. Sharma, R. K. Gangwar, and M. S. Sharawi, "FSS-based spatially decoupled back-to-back four-port MIMO DRA with multidirectional pattern diversity," *IEEE Antennas Wireless Propag. Lett.*, vol. 18, pp. 1552–1556, 2019, doi: 10.1109/LAWP.2019.2922276.

[3] D. Gesbert, M. Shafi, D.-s. Shiu, P. J. Smith, and A. Naguib, "From theory to practice: An overview of MIMO space-time coded wireless systems," *IEEE J. Sel. Areas Commun.*, vol. 21, no. 3, pp. 281–302, Apr. 2003, doi: 10.1109/JSAC.2003.809458.

[4] M. Li, L. Jiang, and K. L. Yeung, "A general and systematic method to design neutralization lines for isolation enhancement in MIMO antenna arrays," *IEEE Trans. Veh. Technol.*, vol. 69, no. 6, pp. 6242–6253, Jun. 2020, doi: 10.1109/TVT.2020.2984044.

[5] M. Li, B. G. Zhong, and S. W. Cheung, "Isolation enhancement for MIMO patch antennas using near-field resonators as coupling-mode transducers," *IEEE Trans. Antennas Propag.*, vol. 67, no. 2, pp. 755–764, Feb. 2019, doi: 10.1109/TAP.2018.2880048.

[6] C.-D. Xue, X. Y. Zhang, Y. F. Cao, Z. Hou, and C. F. Ding, "MIMO antenna using hybrid electric and magnetic coupling for isolation enhancement," *IEEE Trans. Antennas Propag.*, vol. 65, no. 10, pp. 5162–5170, Oct. 2017, doi: 10.1109/TAP.2017.2738033.

[7] M. A. Sufian, N. Hussain, H. Askari, S. G. Park, K. S. Shin, and N. Kim, "Isolation enhancement of a metasurface-based MIMO antenna using slots and shorting pins," *IEEE Access*, vol. 9, pp. 73533–73543, 2021, doi: 10.1109/ACCESS.2021.3079965.

[8] I. Nadeem and D.-Y. Choi, "Study on mutual coupling reduction technique for MIMO antennas," *IEEE Access*, vol. 7, pp. 563–586, 2019, doi: 10.1109/ACCESS.2018.2885558.

[9] S.-W. Su, C.-T. Lee, and F.-S. Chang, "Printed MIMO-antenna system using neutralization-line technique for wireless USB-dongle applications," *IEEE Trans. Antennas Propag.*, vol. 60, no. 2, pp. 456–463, Feb. 2012, doi: 10.1109/TAP.2011.2173450.

[10] A. A. Megahed, M. Abdelazim, E. H. Abdelhay, and H. Y. M. Soliman, "Sub-6 GHz highly isolated wideband MIMO antenna arrays," *IEEE Access*, vol. 10, pp. 19875–19889, 2022, doi: 10.1109/ACCESS.2022.3150278.

[11] N. Sheriff, S. K. A. Rahim, H. T. Chattha, and T. K. Geok, "Multiport single element MIMO antenna systems: A review," *Sensors*, vol. 23, no. 2, p. 747, Jan. 2023, doi: 10.3390/s23020747.

[12] Q. X. Lai, Y. M. Pan, and S. Y. Zheng, "A self-decoupling method for MIMO antenna array using characteristic mode of ground plane," *IEEE Trans. Antennas Propag.*, vol. 71, no. 3, pp. 2126–2135, Mar. 2023, doi: 10.1109/TAP.2023.3240561.

[13] M. S. Alam, N. Misran, B. Yatim, and M. T. Islam, "Development of electromagnetic band gap structures in the perspective of microstrip antenna design," *Int. J. Antennas Propag.*, vol. 2013, pp. 1–22, Jan. 2013, doi: 10.1155/2013/507158.

[14] A. C. J. Malathi and D. Thiripurasundari, "Review on isolation techniques in MIMO antenna systems," *Indian J. Sci. Technol.*, vol. 9, no. 35, pp. 1–10, Sep. 2016, doi: 10.17485/ijst/2016/v9i35/96704.

[15] M. Li, X. Chen, A. Zhang, W. Fan, and A. A. Kishk, "Split-ring resonator-loaded baffles for decoupling of dual-polarized base station array," *IEEE Antennas Wireless Propag. Lett.*, vol. 19, pp. 1828–1832, 2020, doi: 10.1109/LAWP.2020.3020855.

[16] P. M. Paul, K. Kandasamy, and M. S. Sharawi, "A triband circularly polarized strip and SRR-loaded slot antenna," *IEEE Trans. Antennas Propag.*, vol. 66, no. 10, pp. 5569–5573, Oct. 2018, doi: 10.1109/TAP.2018.2854911.

[17] M. S. Sharawi, M. U. Khan, A. B. Numan, and D. N. Aloi, "A CSRR loaded MIMO antenna system for ISM band operation," *IEEE Trans. Antennas Propag.*, vol. 61, no. 8, pp. 4265–4274, Aug. 2013, doi: 10.1109/TAP.2013.2263214.

[18] A. Alfakhri, "Dual polarization and mutual coupling improvement of UWB MIMO antenna with cross shape decoupling structure," *e-Prime Adv. Electr. Eng., Electron. Energy*, vol. 4, Jun. 2023, Art. no. 100130, doi: 10.1016/j.prime.2023.100130.

[19] M. Alibakhshikenari, F. Babaeian, B. S. Virdee, S. Aïssa, L. Azpilicueta, C. H. See, A. A. Althuwayb, I. Huynen, R. A. Abd-Alhameed, F. Falcone, and E. Limiti, "A comprehensive survey on 'various decoupling mechanisms with focus on metamaterial and metasurface principles applicable to SAR and MIMO antenna systems,'" *IEEE Access*, vol. 8, pp. 192965–193004, 2020, doi: 10.1109/ACCESS.2020.3032826.

[20] M. K. Khandelwal, B. K. Kanaujia, and S. Kumar, "Defected ground structure: Fundamentals, analysis, and applications in modern wireless trends," *Int. J. Antennas Propag.*, vol. 2017, pp. 1–22, Jan. 2017, doi: 10.1155/2017/2018527.

[21] Z. Du and Q. Feng, "Gain improvement and front-to-back ratio enhancement for substrate-integrated magnetoelectric dipole antenna," *IEEE Antennas Wireless Propag. Lett.*, vol. 21, pp. 59–63, 2022, doi: 10.1109/LAWP.2021.3117943.

[22] L. Chang, G. Zhang, and H. Wang, "Triple-band microstrip patch antenna and its four-antenna module based on half-mode patch for 5G 4 × 4 MIMO operation," *IEEE Trans. Antennas Propag.*, vol. 70, no. 1, pp. 67–74, Jan. 2022, doi: 10.1109/TAP.2021.3090572.

[23] H.-H. Tran, N. Hussain, H. C. Park, and N. Nguyen-Trong, "Isolation in dual-sense CP MIMO antennas and role of decoupling structures," *IEEE Antennas Wireless Propag. Lett.*, vol. 21, pp. 1203–1207, 2022, doi: 10.1109/LAWP.2022.3161669.

[24] P. Garg and P. Jain, "Isolation improvement of MIMO antenna using a novel flower shaped metamaterial absorber at 5.5 GHz Wimax band," *IEEE Trans. Circuits Syst. II, Exp. Briefs*, vol. 67, no. 4, pp. 675–679, Apr. 2020, doi: 10.1109/TCSII.2019.2925148.

[25] A. Iqbal, O. A Saraereh, A. Bouazizi, and A. Basir, "Metamaterial-based highly isolated MIMO antenna for portable wireless applications," *Electronics*, vol. 7, no. 10, p. 267, Oct. 2018, doi: 10.3390/electronics7100267.

[26] J. Molins-Benlliure, E. Antonino-Daviu, M. Cabedo-Fabrés, and M. Ferrando-Bataller, "Four-port wide-band cavity-backed antenna with isolating X-shaped block for sub-6 GHz 5G indoor base stations," *IEEE Access*, vol. 9, pp. 80535–80545, 2021, doi: 10.1109/ACCESS.2021.3084852.

[27] K.-L. Wong, Z.-W. Tso, and W.-Y. Li, "Very-wide-band six-port single-patch antenna with six uncorrelated waves for MIMO access points," *IEEE Access*, vol. 10, pp. 69555–69567, 2022, doi: 10.1109/ACCESS.2022.3187553.

[28] J. Molins-Benlliure, E. Antonino-Daviu, M. Cabedo-Fabrés, and M. Ferrando-Bataller, "Design of a 10-port MIMO antenna for 5G/WiFi indoor base station applications," in *Proc. IEEE Int. Symp. Antennas Propag. USNC-URSI Radio Sci. Meeting (AP-S/URSI)*, Jul. 2022, pp. 713–714, doi: 10.1109/AP-S/USNC-URSI47032.2022.9886908.

[29] Y. Qin, L. Zhang, C.-X. Mao, and H. Zhu, "A compact wideband antenna with suppressed mutual coupling for 5G MIMO applications," *IEEE Antennas Wireless Propag. Lett.*, vol. 22, pp. 938–942, 2023, doi: 10.1109/LAWP.2022.3229020.

[30] M. Li and S. Cheung, "A novel calculation-based parasitic decoupling technique for increasing isolation in multiple-element MIMO antenna arrays," *IEEE Trans. Veh. Technol.*, vol. 70, no. 1, pp. 446–458, Jan. 2021, doi: 10.1109/TVT.2020.3045231.

[31] H. H. Tran and N. Nguyen-Trong, "Performance enhancement of MIMO patch antenna using parasitic elements," *IEEE Access*, vol. 9, pp. 30011–30016, 2021, doi: 10.1109/ACCESS.2021.3058340.

[32] P. K. Panda and D. Ghosh, "Isolation and gain enhancement of patch antennas using EMNZ superstrate," *AEU Int. J. Electron. Commun.*, vol. 86, pp. 164–170, Mar. 2018, doi: 10.1016/j.aeue.2018.01.037.

[33] M. M. Hasan, M. T. Islam, S. H. A. Almalki, A. G. Alharbi, H. Alsaif, M. S. Islam, and M. Samsuzzaman, "Polarization insensitive dual band metamaterial with absorptance for 5G sub-6 GHz applications," *Sci. Rep.*, vol. 12, no. 1, pp. 1–20, May 2022, doi: 10.1038/s41598-022-12106-7.

[34] M. Moniruzzaman, M. Tariqul Islam, M. Fais Mansor, M. S. Soliman, N. Misran, and M. Samsuzzaman, "Tuning metallic stub loaded symmetrical resonator based dual band metamaterial absorber for wave shielding from Wi-Fi frequencies," *Alexandria Eng. J.*, vol. 63, pp. 399–414, Jan. 2023, doi: 10.1016/j.aej.2022.07.051.

[35] R. Saleem, M. Bilal, H. T. Chattha, S. Ur Rehman, A. Mushtaq, and M. F. Shafique, "An FSS based multiband MIMO system incorporating 3D antennas for WLAN/WiMAX/5G cellular and 5G Wi-Fi applications," *IEEE Access*, vol. 7, pp. 144732–144740, 2019, doi: 10.1109/ACCESS.2019.2945810.

[36] R. Mondal, P. S. Reddy, D. C. Sarkar, and P. P. Sarkar, "Investigation on MIMO antenna for very low ECC and isolation characteristics using FSS and metal-wall," *AEU Int. J. Electron. Commun.*, vol. 135, Jun. 2021, Art. no. 153708, doi: 10.1016/j.aeue.2021.153708.

[37] H. Huang, "A decoupling method for antennas with different frequencies in 5G massive MIMO application," *IEEE Access*, vol. 8, pp. 140273–140278, 2020, doi: 10.1109/ACCESS.2020.3012665.

[38] J. Zhang, S. Yan, X. Hu, and G. A. E. Vandenbosch, "Mutual coupling suppression for on-body multiantenna systems," *IEEE Trans. Electromagn. Compat.*, vol. 62, no. 4, pp. 1045–1054, Aug. 2020, doi: 10.1109/TEMC.2019.2936679.

[39] M. Ameen, O. Ahmad, and R. K. Chaudhary, "Bandwidth and gain enhancement of triple-band MIMO antenna incorporating metasurface-based reflector for WLAN/WiMAX applications," *IET Microw., Antennas Propag.*, vol. 14, no. 13, pp. 1493–1503, Jul. 2020, doi: 10.1049/iet-map.2020.0350.

[40] D. He, Y. Chen, and S. Yang, "A low-profile triple-band shared-aperture antenna array for 5G base station applications," *IEEE Trans. Antennas Propag.*, vol. 70, no. 4, pp. 2732–2739, Apr. 2022, doi: 10.1109/TAP.2021.3137486.

[41] H. Sakli, C. Abdelhamid, C. Essid, and N. Sakli, "Metamaterial-based antenna performance enhancement for MIMO system applications," *IEEE Access*, vol. 9, pp. 38546–38556, 2021, doi: 10.1109/ACCESS.2021.3063630.

[42] R. J. Langley and E. A. Parker, "Equivalent circuit model for arrays of square loops," *Electron. Lett.*, vol. 18, no. 7, p. 294, Jan. 1982, doi: 10.1049/el:19820201.

[43] R. Mittra, C. H. Chan, and T. Cwik, "Techniques for analyzing frequency selective surfaces—A review," *Proc. IEEE*, vol. 76, no. 12, pp. 1593–1615, Dec. 1988, doi: 10.1109/5.16352.

[44] A. R. Varkani, Z. H. Firouzeh, and A. Z. Nezhad, "Equivalent circuit model for array of circular loop FSS structures at oblique angles of incidence," *IET Microw., Antennas Propag.*, vol. 12, no. 5, pp. 749–755, Feb. 2018, doi: 10.1049/iet-map.2017.1004.

[45] Y. Yuan, X. Xi, and Y. Zhao, "Compact UWB FSS reflector for antenna gain enhancement," *IET Microw., Antennas Propag.*, vol. 13, no. 10, pp. 1749–1755, May 2019, doi: 10.1049/iet-map.2019.0083.

[46] J. Kulkarni, A. Desai, and C.-Y.-D. Sim, "Wideband four-port MIMO antenna array with high isolation for future wireless systems," *AEU Int. J. Electron. Commun.*, vol. 128, Jan. 2021, Art. no. 153507, doi: 10.1016/j.aeue.2020.153507.

[47] B. C. Pan and T. J. Cui, "Broadband decoupling network for dual-band microstrip patch antennas," *IEEE Trans. Antennas Propag.*, vol. 65, no. 10, pp. 5595–5598, Oct. 2017, doi: 10.1109/TAP.2017.2742539.

[48] A. Alieldin, Y. Huang, S. J. Boyes, M. Stanley, S. D. Joseph, Q. Hua, and D. Lei, "A triple-band dual-polarized indoor base station antenna for 2G, 3G, 4G and Sub-6 GHz 5G applications," *IEEE Access*, vol. 6, pp. 49209–49216, 2018, doi: 10.1109/ACCESS.2018.2868414.

[49] S. Padmanathan, A. Abdullah Al-Hadi, A. M. Elshirkasi, S. S. Al-Bawri, M. T. Islam, T. Sabapathy, M. Jusoh, P. Akkaraekthalin, and P. J. Soh, "Compact multiband reconfigurable MIMO antenna for sub-6 GHz 5G mobile terminal," *IEEE Access*, vol. 10, pp. 60241–60252, 2022, doi: 10.1109/ACCESS.2022.3180048.

[50] M. Elahi, A. Altaf, E. Almajali, and J. Yousaf, "Mutual coupling reduction in closely spaced MIMO dielectric resonator antenna in H-plane using closed metallic loop," *IEEE Access*, vol. 10, pp. 71576–71583, 2022, doi: 10.1109/ACCESS.2022.3187433.

[51] K.-L. Wong, X.-Q. Ye, and W.-Y. Li, "Wideband four-port single-patch antenna based on the quasi-$TM_{1/2,1/2}$ mode for 5G MIMO access-point application," *IEEE Access*, vol. 10, pp. 9232–9240, 2022, doi: 10.1109/ACCESS.2022.3144231.

[52] G. Saxena, S. Kumar, S. Chintakindi, A. Al-Tamim, M. H. Abidi, W. A. M. Saif, S. Kansal, R. Jain, S. Singh, A. K. Dohare, P. K. Maduri, M. Kumar, H. Singh, and Y. K. Awasthi, "Metasurface instrumented high gain and low RCS X-band circularly polarized MIMO antenna for IoT over satellite application," *IEEE Trans. Instrum. Meas.*, vol. 72, pp. 1–10, 2023, doi: 10.1109/TIM.2023.3287241.

[53] S. Tariq, S. I. Naqvi, N. Hussain, and Y. Amin, "A metasurface-based MIMO antenna for 5G millimeter-wave applications," *IEEE Access*, vol. 9, pp. 51805–51817, 2021, doi: 10.1109/ACCESS.2021.3069185.

[54] A. C. K. Mak, C. R. Rowell, and R. D. Murch, "Isolation enhancement between two closely packed antennas," *IEEE Trans. Antennas Propag.*, vol. 56, no. 11, pp. 3411–3419, Nov. 2008, doi: 10.1109/TAP.2008.2005460.

[55] D. M. Pozar, *Microwave Engineering*, 4th ed. Hoboken, NJ, USA: Wiley, 2011.

[56] C. A. Balanis, *Antenna Theory Analysis and Design*, 4th ed. Hoboken, NJ, USA: Wiley, 2016.

[57] R. A. Abdulhasan, R. Alias, K. N. Ramli, F. C. Seman, R. A. Abd-Alhameed, and Y. A. Jawhar, "Directional and isolated UWB-MIMO antenna-based uniplanar UWB-FSS array and T-strip for bi-static microwave imaging: Baggage-scanner," *Int. J. RF Microw. Comput.-Aided Eng.*, vol. 32, no. 2, Nov. 2021, Art. no. e22960, doi: 10.1002/mmce.22960.

[58] A. Desai, J. Kulkarni, M. M. Kamruzzaman, Š. Hubálovský, H.-T. Hsu, and A. A. Ibrahim, "Interconnected CPW fed flexible 4-port MIMO antenna for UWB, X, and Ku band applications," *IEEE Access*, vol. 10, pp. 57641–57654, 2022, doi: 10.1109/ACCESS.2022.3179005.

[59] M. Alibakhshikenari, M. Khalily, B. S. Virdee, C. H. See, R. A. Abd-Alhameed, and E. Limiti, "Mutual coupling suppression between two closely placed microstrip patches using EM-bandgap metamaterial fractal loading," *IEEE Access*, vol. 7, pp. 23606–23614, 2019, doi: 10.1109/ACCESS.2019.2899326.

M. Y. ZEAIN was born in Baghdad, Iraq, in 1989. He received the B.Sc. degree in computer engineering from Al Maarif University College (AUC) and the M.Sc. degree in electronic and computer engineering with majors in telecommunication engineering from Universiti Teknikal Malaysia Melaka (UTeM), Malaysia, in 2017, where he is currently pursuing the Ph.D. degree in electronic and computer technology and engineering. His research interests include antenna applications, wideband antenna, multiple-input and multiple-output (MIMO) antenna, 5G antenna, and frequency-selective surface (FSS).

MAISARAH ABU received the bachelor's degree in electrical engineering from Universiti Teknologi MARA, in 2001, the master's degree from Universiti Kebangsaan Malaysia, in 2003, and the Ph.D. degree from Universiti Teknologi Malaysia, in 2012, with a focus on dipole antenna and artificial magnetic conductor for RFID application. Since 2003, she has been a Lecturer with Universiti Teknikal Malaysia Melaka (UTeM), where she is currently an Assistant Professor. Her research interests include RF, microwave and antenna with metamaterial (EBG, AMB, and FSS), and RFID.

AYMAN A. ALTHUWAYB (Member, IEEE) received the B.Sc. degree (Hons.) in electrical engineering (electronics and communications) from Jouf University, Saudi Arabia, the M.Sc. degree in electrical engineering from California State University, Fullerton, CA, USA, in 2015, and the Ph.D. degree in electrical engineering from Southern Methodist University, Dallas, TX, USA, in 2018. He is currently an Assistant Professor with the Department of Electrical Engineering, Jouf University. His current research interests include antenna design and propagation, microwaves and millimeter-waves, wireless power transfer, ultra-wideband, and multiband antenna, filters, and others.

HUSSEIN ALSARIERA was born in Mu'tah, Jordan, in 1985. He received the B.Eng. degree in electronic and telecommunication engineering from Misr University for Science and Technology (MUST), in 2010, and the master's degree in telecommunication engineering from Universiti Teknikal Malaysia Melaka (UTeM), in 2015, where he is currently pursuing the Ph.D. degree with the Faculty of Electronic and Computer Technology and Engineering (FTKEK), with a focus on monopole antennas.

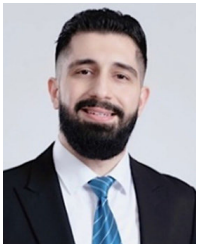

AHMED JAMAL ABDULLAH AL-GBURI (Senior Member, IEEE) received the M.Eng. and Ph.D. degrees in electronics and computer engineering (telecommunication systems) from Universiti Teknikal Malaysia Melaka (UTeM), Malaysia, in 2017 and 2021, respectively. From December 2021 to March 2023, he was a Postdoctoral Fellow with the Microwave Research Group (MRG), UTeM. He is currently a Senior Lecturer with the Faculty of Electrical and Electronic Engineering Technology (FTKEE), UTeM. He has authored and coauthored numerous papers in journals and conference proceedings. His research interests include microwave sensors, metasurfaces, UWB antennas, array antennas, and miniaturized antennas for UWB and 5G applications. He is a member of the Board of Engineers Malaysia (BEM) and the International Association of Engineers (IAENG). He was awarded the Best Paper Award from the IEEE Community and has earned several gold, silver, and bronze medals in international and local competitions. In 2023, he was recognized as one of the top 2% scientists worldwide by Stanford University and published by Elsevier.

ALI ABDULATEEF ABDULBARI received the B.S. degree in computer and electrical engineering from Iraq, in 2014, the M.Sc. degree in communication engineering from Universiti Teknikal Malaysia Melaka (UTeM), in 2018, and the Ph.D. degree in communication engineering from Universiti Teknologi Malaysia (UTM), in 2023. He is currently a member of staff with the Information Technology Center, University of Technology, Iraq, Baghdad, Iraq. His main research interests include multibeam antenna array with a Butler matrix beamforming network for 5G wireless communications.

ZAHRILADHA ZAKARIA (Senior Member, IEEE) was born in Johor, Malaysia. He received the B.Eng. and M.Eng. degrees in electrical and electronic engineering from Universiti Teknologi Malaysia, Malaysia, in 1998 and 2004, respectively, and the Ph.D. degree in electrical and electronic engineering from the Institute of Microwaves and Photonics (IMP), University of Leeds, Leeds, U.K., in 2010. From 1998 to 2002, he was with STMicroelectronics, Malaysia, where he was a Product Engineer. He is currently a Professor with the Microwave Research Group (MRG), Faculty of Electronic and Computer Engineering, Universiti Teknikal Malaysia Melaka (UTeM), where he teaches microwave engineering, antenna and propagation, electronic systems, communication principles, wireless communications, and signal processing. He also investigates energy harvesting, sensor, and data communications for interdisciplinary applications. He has published more than 300 scientific papers in journals, proceedings, and book chapters. He holds eight intellectual property rights. His research interests include a variety of microwave device developments, such as planar and non-planar microwave filters, resonators, amplifiers, and antennas. He was a recipient of the Top Research Scientist Malaysia (TRSM), in 2021. He has won several awards, including gold medal during several research and innovation exhibitions at the national and international level, such as the UTeMEX 2012, 2013, and 2015, Malaysia Technology Expo (MTE 2012–2014 and 2016), ITEX 2016 and 2017, International Trade Fair Ideas Inventions New Products (iENA 2012), Nuremberg, Germany, and Seoul International Invention Fair (SiiF 2013, 2016, 2017, and 2019), Seoul, South Korea. He is an Active Reviewer for prominent journals, such as IEEE TRANSACTIONS ON MICROWAVE THEORY AND TECHNIQUES (MTT), IEEE SENSOR, IEEE ACCESS, IEEE MICROWAVE AND WIRELESS COMPONENTS LETTERS (MWCL), and *IET Microwave, Antennas and Propagation*.